

NAMING TO LEARN: CLASS INCREMENTAL LEARNING FOR VISION-LANGUAGE MODEL WITH UNLABELED DATA

Qiwei Li¹, Xiaochen Yang² & Jiahuan Zhou^{1*}

¹Wangxuan Institute of Computer Technology, Peking University

²Harbin Institute of Technology

{lqw, jiahuanzhou}@pku.edu.cn, 2022211854@stu.hit.edu.cn

ABSTRACT

Class Incremental Learning (CIL) enables models to adapt to evolving data distributions by learning new classes over time without revisiting previous data. While recent methods utilizing pre-trained models have shown promising results, they often assume access to fully labeled data for each incremental task, which is often impractical. In this paper, we instead tackle a more realistic scenario in which only unlabeled data and the class-name set are available for each new class. Although one could generate pseudo labels with a vision-language model and apply existing CIL methods, the inevitable noise in these pseudo labels tends to aggravate catastrophic forgetting. To overcome this challenge, we propose a method named N2L employing a regression objective with mean squared error loss, which can be solved in a recursive manner. To refine the pseudo labels, N2L applies feature dimensionality reduction to the extracted image features and iteratively updates the labels using a classifier trained on these reduced features. Furthermore, a bi-level weight adjustment strategy is proposed to downweight low-confidence pseudo labels via intra-class adjustment and compensate for pseudo-label class imbalance through inter-class adjustment. This incremental learning with adjustment can be solved recursively, yielding identical performance to joint training with unlabeled data and thereby mitigating forgetting. Our theoretical analysis supports the effectiveness of the pseudo label refinement process, and experiments on various datasets demonstrate that our proposed method outperforms SOTA methods. Code is available at <https://github.com/zhoujiahuan1991/ICLR2026-N2L>

1 INTRODUCTION

Class Incremental learning (CIL) (Zhou et al., 2024c;a; Wang et al., 2024), has attracted sustained attention in recent years due to its ability to adapt models to continuously evolving data scenarios, enabling lifelong learning capabilities. In the CIL setting, new classes are introduced sequentially, and the model must learn them without direct access to previously seen data, while maintaining a unified model capable of recognizing all encountered classes. The core challenge lies in mitigating catastrophic forgetting (French, 1999), a phenomenon where newly acquired knowledge overwrites and degrades previously learned information.

Recent advances in CIL utilizing pre-trained model-based method (Zhou et al., 2024a), such as Vision Transformers (ViT (Dosovitskiy et al., 2021)) and Contrastive Language-Image Pretraining (CLIP (Radford et al., 2021)), have shown promising performance in CIL. Leveraging their rich prior knowledge, these methods achieve competitive performance by fine-tuning only classification heads and a subset of parameters. However, they typically assume fully labeled data for all incremental tasks which is often impractical in real-world applications where annotations are scarce or costly. To address this, as shown in Fig. 1, we propose a more realistic class incremental learning paradigm: at each incremental task, the model receives *only class names and unlabeled data* for each category.

*Corresponding author.

A straightforward solution is to exploit a pre-trained vision-language model: convert each class name into its textual embedding, compute similarities between image and text embeddings, and use the highest-scoring class as a pseudo label for each image. However, these pseudo labels are inherently noisy, which degrades performance and exacerbates forgetting.

To address these challenges, we propose N2L, a method for CIL with frozen vision-language models and unlabeled data. Inspired by analytic CIL (Zhuang et al., 2022), N2L adopts a mean squared error regression objective instead of the standard cross-entropy loss, which has been shown to be more robust to noisy labels (Ghosh et al., 2017). Prior work (Zhuang et al., 2022) has demonstrated that combining such a regression loss with a recursive update scheme in an incremental setting, effectively mitigating forgetting. Building on this foundation, we first develop a novel pseudo label refinement mechanism. Unlike previous method (Xu et al., 2024) that increases feature dimensionality, our method applies feature dimensionality reduction and trains a label refinement classifier on the reduced features to iteratively update the pseudo labels. We further provide theoretical guarantees for the effectiveness of this procedure. Additionally, N2L incorporates a bi-level weight adjustment strategy: inter-class adjustment to address class imbalance introduced by noisy pseudo labels, and intra-class adjustment to downweight low-confidence samples that are more likely to be mislabeled. Finally, we derive a recursive formulation of regression with weight adjustment, ensuring performance identical to joint training with unlabeled data and alleviating forgetting.

In summary: (1) We propose a practical class incremental learning setting in which only unlabeled data and class names are available at each task. (2) We propose a feature dimensionality reduction-based pseudo label refinement method, supported by theoretical analysis. (3) We design inter-class and intra-class adjustment schemes to compensate for pseudo-label class imbalance and incorporate confidence information from noisy pseudo labels. (4) Experiments on various benchmarks demonstrate that N2L outperforms state-of-the-art approaches by a large margin.

2 RELATED WORK

2.1 CLASS INCREMENTAL LEARNING

Class incremental learning methods can be broadly categorized into three directions: parameter regularization, exemplar replay, and architectural expansion. Regularization-based methods introduce additional constraints to limit changes in model parameters (Aljundi et al., 2018; Kirkpatrick et al., 2017) or intermediate representations (Li & Hoiem, 2017; Zhang et al., 2020; Kang et al., 2022; Li et al., 2024a), aiming to preserve performance without accessing previous data. Replay-based approaches typically store representative samples or features from previous learned classes. Some works focus on selecting more effective samples (Sun et al., 2023; Liu et al., 2020; Lopez-Paz & Ranzato, 2017), while others investigate how to and utilize the feature representation of each classes (Zhu et al., 2021; Toldo & Ozay, 2022; Li et al., 2024b). Architecture-based methods (Douillard et al., 2022; Wang et al., 2022a; Hu et al., 2023) dynamically expand model capacity by introducing new parameter modules for new classes while keeping existing parameters fixed.

2.2 PRE-TRAINED MODEL BASED CIL

Recent CIL research leverages pre-trained models due to their rich prior knowledge. These methods typically adopt parameter-efficient fine-tuning (PEFT) to adapt to new tasks while keeping the backbone frozen. A large portion of these methods build on ViT. Some works (Wang et al., 2022c;b; Smith et al., 2023; Wang et al., 2023; Li & Zhou, 2025) introducing learnable prompt parameters along with corresponding prompt selection or weighting strategies. While others employ LoRA (Liang & Li,

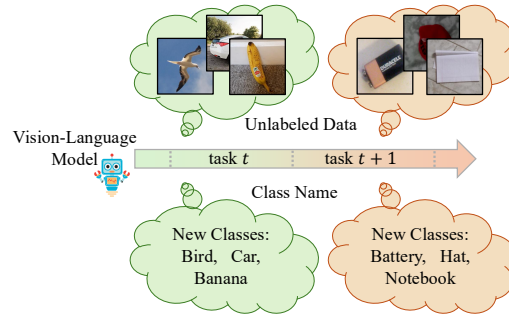


Figure 1: Class incremental learning for vision-language model with unlabeled data.

2024; Wu et al., 2025) or Adapter (Tan et al., 2024; Zhou et al., 2024b) to achieve efficient adaptation. More recently, there has been growing interest in using CLIP as the backbone, motivated by its strong multimodal capabilities and generalization performance. Several studies (Zheng et al., 2023; 2024; Gao et al., 2024; Yu et al., 2024) aim to preserve CLIP’s generalization while adapting to new tasks via parameter regularization or task identification mechanisms. Other approaches (Huang et al., 2024; Zhou et al., 2025a) leverage CLIP’s image-text alignment capability to maintain knowledge of old classes and enhance discrimination of new classes through textual guidance or task adaptation techniques. Additionally, some replay-based methods (Zhou et al., 2025b; Jha et al., 2024) improve inter-class feature consistency under limited exemplar budgets using probabilistic modeling or task-specific module expansion. However, all these methods assume that accurate label is available for each training sample, which can be labor-intensive.

2.3 LEARNING FROM UNLABELED DATA

In many real world scenarios, category labels are scarce, and the majority of available data is unlabeled, creating a demand for effective learning from unlabeled data. Pseudo labeling methods (Lee et al., 2013; Rasmus et al., 2015; Sohn et al., 2020) have been widely used to address this challenge. In the context of vision-language models, UPL (Huang et al., 2022) proposes generating more reliable pseudo labels by selecting multiple examples with the highest confidence for each class. LaFTer (Mirza et al., 2023) generates pseudo labels by training a pure text classifier on a corpus of text data generated by a large language model. CPL (Zhang et al., 2024) introduces a candidate pseudo label generation strategy that select reliable pseudo labels by intra-instance and inter-instance confidence score. However, these methods assume a static learning scenario where all data is provided at once. In this paper, we propose a new setting, class incremental learning with unlabeled data, in which the model must continuously acquire new knowledge from unlabeled data while mitigating forgetting of previously learned information.

3 METHOD

3.1 PRELIMINARIES

Problem definition. CIL with vision-language models considers the scenario where a pre-trained model, such as CLIP, composing an image encoder and a text encoder $\mathcal{V} = (f_{\text{img}}, f_{\text{text}})$, learns from a sequence of tasks $\{\mathcal{T}_1, \mathcal{T}_2, \dots, \mathcal{T}_T\}$. Each task \mathcal{T}_t introduces a disjoint set of classes \mathcal{Y}_t , satisfying $\mathcal{Y}_i \cap \mathcal{Y}_j = \emptyset$ for $i \neq j$. At each task t , the model is trained with new data \mathcal{D}_t but has no access to previously seen datasets $\mathcal{D}_1, \dots, \mathcal{D}_{t-1}$. The goal is to update the model to recognize all classes seen so far while mitigating catastrophic forgetting. In this work, we address a more realistic and challenging setting in which n_t unlabeled samples, $\mathcal{U}_t = \{x_j\}_{j=1}^{n_t}$, and a corresponding class name set $\mathcal{C}_t = \{c_y | y \in \mathcal{Y}_t\}$ are available. Hence, the dataset at task t is defined as $\mathcal{D}_t = \{\mathcal{U}_t, \mathcal{C}_t\}$.

3.2 OVERVIEW

As shown in Fig. 2, the overall pipeline of N2L during task t has four steps: (1) Pseudo Label Generation. Using the zero-shot capability of the pre-trained vision-language model, pseudo labels, $\tilde{\mathbf{Y}}_t$, are assigned to unlabeled images based on the similarity between visual and textual features. (2) Progressive Label Refinement. We apply feature dimensionality reduction to the extracted image features \mathbf{X}_t of task t , obtaining a reduced representation $\mathbf{X}_{t,k}$. The pseudo label is iteratively updated by a label refinement classifier, $\hat{\mathbf{W}}'_t$, which is learned using the reduced representation and pseudo label with the objective of regression. (3) Bi-level Weight Adjustment. To compensate for pseudo-label class imbalance and utilize the confidence information of samples, we propose a bi-level weight adjustment strategy. A recursive solution is derived for learning with weight adjustment. (4) Finally, an incremental classifier, $\hat{\mathbf{W}}_t$ is learned using full features \mathbf{X} , updated label $\tilde{\mathbf{Y}}'_t$.

3.3 ANALYTIC CIL WITH UNLABELED DATA

Pseudo Label Generation. The absence of labels necessitates reliable pseudo-labeling to associate each image with a class. Leveraging the zero-shot capabilities of a pre-trained vision-language model

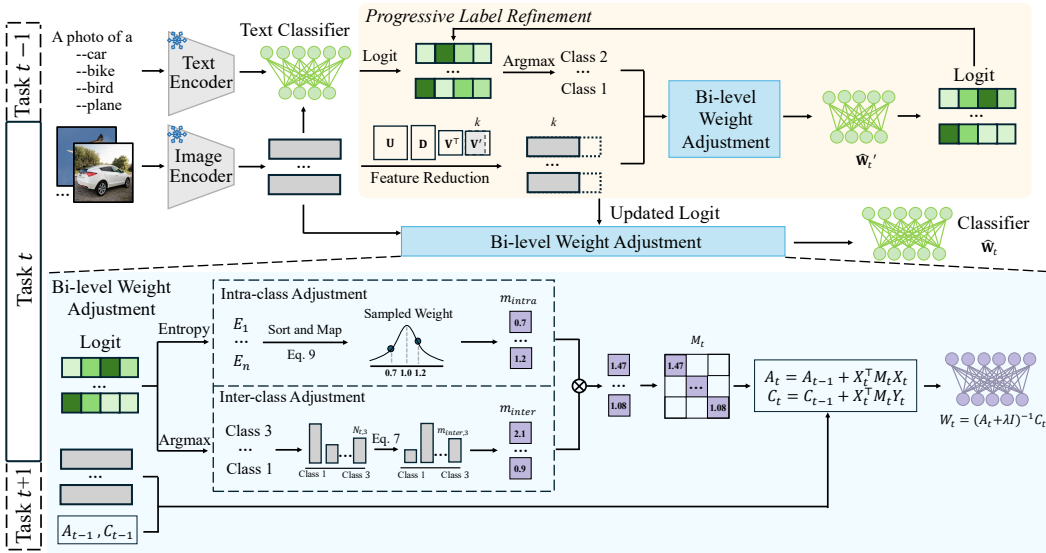


Figure 2: Overview of N2L during task t . First, each unlabeled image is assigned a pseudo label using CLIP. To refine these noisy labels, feature dimensionality reduction is applied to the extracted features, and the pseudo labels are iteratively updated using a label refinement classifier $\hat{\mathbf{W}}'_t$ learned by a regression objective. Meanwhile, intra-class and inter-class adjustment strategies are introduced to leverage sample confidence and address class imbalance. Finally, the incremental classifier $\hat{\mathbf{W}}_t$ is learned using the updated pseudo labels and the weight adjustment strategy.

(e.g., CLIP), we generate a pseudo label \tilde{y}_i for each unlabeled image $x_i \in \mathcal{U}_t$ based on the similarity between visual and textual features:

$$\tilde{y}_i = \arg \max_{c \in \mathcal{C}_t} \langle f_{\text{img}}(x_i), f_{\text{text}}(p_c) \rangle, \quad (1)$$

p_c is the prompt for class c (e.g., “a photo of a [CLASS]”).

While this approach enables CIL without annotations, the generated pseudo labels are often noisy. Although applying cross-entropy loss is the common approach for classification tasks, existing method (Ghosh et al., 2017) has shown that mean squared error (MSE) loss is more robust to noise. Recent studies in CIL (Zhuang et al., 2022; Xu et al., 2024; Zhuang et al., 2024; Fang et al., 2024) further demonstrate that using MSE loss along with a recursive update of the classifier achieves performance comparable to joint training, effectively mitigating forgetting.

Analytic CIL. Given extracted features of unlabeled data of task 1 to T , $\mathbf{X}_{1:T}$, (each row consists of a image feature, $f_{\text{img}}(x)$, for the unlabeled data x) and one-hot label tensor $\mathbf{Y}_{1:T}$, the training objective of joint training on all tasks is formed as ridge regression (Zhuang et al., 2022):

$$\mathcal{L}(\mathbf{W}_T) = \|\mathbf{X}_{1:T}\mathbf{W}_T - \mathbf{Y}_{1:T}\|_F^2 + \lambda \|\mathbf{W}_T\|_F^2. \quad (2)$$

The closed-form solution of \mathbf{W}_T is:

$$\hat{\mathbf{W}}_T = \arg \min_{\mathbf{W}_T} \mathcal{L}(\mathbf{W}_T) = (\mathbf{A}_T + \lambda \mathbf{I})^{-1} \mathbf{C}_T, \quad (3)$$

where matrix \mathbf{A}_T and \mathbf{C}_T can be calculated in an recursive form, with \mathbf{A}_0 and \mathbf{C}_0 are initialized as zero matrices:

$$\mathbf{A}_t = \mathbf{A}_{t-1} + \mathbf{X}_t^\top \mathbf{X}_t, \quad \mathbf{C}_t = \mathbf{C}_{t-1} + \mathbf{X}_t^\top \mathbf{Y}_t. \quad (4)$$

Then, by obtaining and updating the matrix \mathbf{A}_t and \mathbf{C}_t during the training of each task t , the final classifier $\hat{\mathbf{W}}_T$ converges to the *same solution as that obtained through joint training*. The derivation is provided in Appendix F.

3.4 PROGRESSIVE LABEL REFINEMENT

In the task of CIL with unlabeled data, the pseudo label generated by zero-shot CLIP can be noisy, and to tackle this problem, we propose a label refinement method based on the dimensionality-reduced features. For the task t , we first apply singular value decomposition (SVD) to the extracted feature matrix with feature dimension d , $\mathbf{X}_t = \mathbf{UDV}^\top$, where $\mathbf{X}_t \in \mathbb{R}^{n_t \times d}$, $\mathbf{U} \in \mathbb{R}^{n_t \times n_t}$, $\mathbf{V} = [\mathbf{v}_1, \dots, \mathbf{v}_d] \in \mathbb{R}^{d \times d}$. The i -th diagonal elements of \mathbf{D} is d_i . We select the top- k singular vectors $\mathbf{V}_k = [\mathbf{v}_1, \dots, \mathbf{v}_k]$ whose singular values are above the threshold θ , and project the features as: $\mathbf{X}_{t,k} = \mathbf{X}_t \mathbf{V}_k \in \mathbb{R}^{n_t \times k}$. We then perform regression using the reduced features $\mathbf{X}_{k,t}$ and pseudo label $\tilde{\mathbf{Y}}_t$ to obtain a refining classifier $\hat{\mathbf{W}}'_t$. The refined pseudo labels are computed as:

$$\tilde{\mathbf{Y}}'_t = \arg \max \mathbf{X}_{t,k} \hat{\mathbf{W}}'_t. \quad (5)$$

This process is iterated several times to progressively refine the pseudo labels.

We provide a theoretical guarantee for the effectiveness of our pseudo label refinement method:

Theorem 1. Consider the regression model with noisy labels: $\mathbf{y} = \mathbf{X}\mathbf{w}^* + \boldsymbol{\varepsilon}$, where features are $\mathbf{X} \in \mathbb{R}^{n \times d}$, $\mathbf{w}^* \in \mathbb{R}^d$ is the true regression coefficient vector, and $\boldsymbol{\varepsilon}$ is the noise with zero mean and variance σ^2 . Let the SVD of $\mathbf{X} = \mathbf{UDV}^\top$, $\mathbf{V} = [\mathbf{v}_1, \dots, \mathbf{v}_d]$. α_i is the i -th coordinate of vector $\boldsymbol{\alpha}^* = \mathbf{V}^\top \mathbf{w}^*$.

If $\sigma^2 \geq (2\lambda + d_j^2)(\alpha_j^*)^2$, projecting \mathbf{X} onto the eigenvectors without j -th components (denoted $\mathbf{X}' = \mathbf{UDV}'^\top$) yields a smaller expected mean squared error:

$$\mathbb{E} [\|\mathbf{X}'\hat{\mathbf{w}}' - \mathbf{X}\mathbf{w}^*\|_F^2] \leq \mathbb{E} [\|\mathbf{X}\hat{\mathbf{w}} - \mathbf{X}\mathbf{w}^*\|_F^2], \quad (6)$$

where $\hat{\mathbf{w}}$ and $\hat{\mathbf{w}}'$ are the regression solutions using \mathbf{X} and \mathbf{X}' , $\mathbf{V}' = [\mathbf{v}_1, \dots, \mathbf{v}_{j-1}, \mathbf{v}_{j+1}, \dots, \mathbf{v}_d]$, λ is the regularization hyperparameter in ridge regression, typically set to 0.1.

Proof. Provided in Appendix. E.1.

In this theorem, α_j^* represents how much of the \mathbf{w}^* lies in the j -th singular direction of \mathbf{X} , and d_j is the singular value corresponding to that direction. This theorem implies that when α_j^* is small (little true signal) or d_j is small (poor information of \mathbf{X} contained in the j -th direction), the model is more likely to overfit noise in that direction. Then, including this direction harms rather than helps.

In practice (Appendix. E.2), we empirically observe that $\sigma^2 \leq 2\lambda(\alpha_i^*)^2$ for most α_i^* . This leads to a threshold of $\theta = \sqrt{\frac{\sigma^2}{(\alpha_i^*)^2} - 2\lambda}$. In our experiments, we use $\theta = 10$, and k in Eq.5 corresponds to the largest index such that the singular value $d_k \geq \theta$. Analysis for different values of θ is provided in Fig.5.

3.5 BI-LEVEL WEIGHT ADJUSTMENT

Although the pseudo labels generated by the pre-trained vision-language model are refined using the proposed method, the learning process still faces two challenges: (1) The number of samples per class predicted by pseudo label varies, which hinders the learning of the minor classes. (2) The pseudo labels are hard 0-1 labels obtained via the argmax operation, which discards useful confidence information embedded in the soft predictions. To address these issues, we propose a weight adjustment strategy, which consists of two components: **inter-class adjustment** and **intra-class adjustment**, allowing dynamic weight assignment to individual samples.

Inter-class Adjustment. For task t , given n_t samples with features \mathbf{X}_t and their corresponding pseudo labels $\tilde{\mathbf{Y}}'_t$, let $N_{t,i}$ denotes the number of samples belong to class c_i . To balance the samples from different classes, we define an adjustment factor $m_{inter} \in \mathbb{R}^{n_t}$ as:

$$m_{inter,i} = \frac{n_t}{N_{t,i} * |\mathcal{C}_t|}. \quad (7)$$

This ensures that the total weight assigned to each class is normalized to $\frac{n_t}{|\mathcal{C}_t|}$, effectively balancing different classes during training.

Table 1: Comparison of different methods. Best scores are in **bold**. The second-best scores are in underline.

Method	Aircraft				Cars				CIFAR100			
	B0Inc10		B50Inc10		B0Inc10		B50Inc10		B0Inc10		B50Inc10	
	$\bar{\mathcal{A}}$	\mathcal{A}_B										
ZS-CLIP	26.61	17.16	21.66	17.16	82.90	76.73	78.74	76.73	81.81	71.38	76.49	71.38
Label	66.38	56.31	59.18	56.31	93.57	89.15	90.92	89.14	88.52	81.92	85.23	81.92
CODA-Prompt	26.56	17.79	18.11	12.28	79.69	69.03	67.81	56.59	79.36	67.74	66.94	54.64
MoE-Adapter	26.73	17.92	22.19	17.52	83.16	77.02	79.21	77.72	81.86	71.53	76.57	71.49
RAPF	29.07	19.52	20.83	18.46	83.77	73.26	75.73	71.56	84.47	76.08	77.30	74.33
RAIL	<u>36.23</u>	<u>33.59</u>	23.75	<u>25.99</u>	<u>88.64</u>	<u>84.68</u>	<u>82.72</u>	<u>82.13</u>	<u>87.34</u>	<u>80.37</u>	<u>81.44</u>	<u>78.89</u>
ENGINE	34.77	25.41	<u>26.94</u>	23.56	86.90	78.76	82.67	79.93	85.15	77.11	79.89	76.15
N2L	43.73	40.21	29.69	32.42	92.38	87.50	86.42	85.45	87.80	81.13	82.92	80.30
CUB												
Method	B0Inc20		B100Inc20		B0Inc20		B100Inc20		B0Inc10		B50Inc10	
	$\bar{\mathcal{A}}$	\mathcal{A}_B										
	75.47	63.72	69.06	63.72	38.43	26.43	31.12	26.43	75.88	67.79	71.68	67.79
Label	86.43	79.05	82.29	79.06	53.18	45.27	49.71	45.26	98.74	97.75	98.37	97.75
CODA-Prompt	67.40	51.91	53.24	37.64	38.25	26.23	26.22	19.22	81.61	75.18	67.06	58.87
MoE-Adapter	73.69	63.07	68.29	63.09	40.14	28.70	32.45	28.53	75.35	67.36	72.28	69.07
RAPF	72.08	58.14	62.27	56.02	39.16	25.88	28.93	24.70	85.99	81.10	75.70	74.31
RAIL	<u>81.64</u>	<u>73.93</u>	<u>73.08</u>	<u>70.91</u>	39.80	<u>35.13</u>	31.21	<u>30.19</u>	<u>90.18</u>	<u>89.90</u>	81.05	<u>84.27</u>
ENGINE	77.06	65.07	70.85	64.92	<u>44.57</u>	31.24	<u>34.62</u>	29.96	87.85	84.46	<u>82.30</u>	81.04
N2L	83.41	76.48	75.16	73.40	49.31	41.59	41.42	38.65	95.00	93.29	86.41	87.87

Intra-class Adjustment. To incorporate prediction confidence, we propose an intra-class adjustment strategy based on entropy of the logit. For task t , given the logits $\mathbf{X}_{t,k} \hat{\mathbf{W}}'_t$ (as described in Eq. 5), we compute the entropy for each sample, yielding $\mathbf{E} = (E_1, \dots, E_{n_t})$. A lower entropy indicates higher confidence, suggesting that such samples should be weighted more heavily. While a naive choice might be $\frac{1}{\mathbf{E}}$, this risks numerical instability when entropy values are close to zero. Additionally, variations in entropy across different datasets make it challenging for a single function to generalize effectively. Instead, we sample weights from a gaussian distribution $\mathcal{N}(1, \sigma^2)$ and sort them in ascending order.

$$m'_1, m'_2, \dots, m'_{n_t} \sim \mathcal{N}(1, \sigma^2), \quad (8)$$

where $m'_1 \leq m'_2 \leq \dots \leq m'_{n_t}$. Then we rearrange the weight according to the order of the entropy:

$$m_{intra,i} = m'_{(\text{rank}(E_i))}, \quad (9)$$

where, $\text{rank}(E_i)$ denotes the position of E_i among \mathbf{E} when the values are sorted in descending order. Further analysis is provided in Table.3 in experiment section.

Finally, the weight for the i -th sample is computed as:

$$m_i = m_{intra,i} * m_{inter,i}. \quad (10)$$

Analytic CIL with Weight Adjustment. With the computed weights, the optimization objective (Eq. 2) is reformed as:

$$(\mathbf{X}_{1:T} \mathbf{W}_T - \mathbf{Y}_{1:T})^\top \mathbf{M} (\mathbf{X}_{1:T} \mathbf{W}_T - \mathbf{Y}_{1:T}) + \lambda \|\mathbf{W}_T\|_F^2, \quad (11)$$

where $\mathbf{M} = \text{diag}(\mathbf{M}_1, \dots, \mathbf{M}_T)$. \mathbf{M}_t is the diagonal weight matrix for task t , whose diagonal elements are m_i . The closed-form solution for \mathbf{W}_T can be recursively calculated:

$$\hat{\mathbf{W}}_T = \arg \min_{\mathbf{W}_T} \mathcal{L}(\mathbf{W}_T) = (\mathbf{A}_T + \lambda \mathbf{I})^{-1} \mathbf{C}_T, \quad (12)$$

with

$$\mathbf{A}_t = \mathbf{A}_{t-1} + \mathbf{X}_t^\top \mathbf{M}_t \mathbf{X}_t, \quad \mathbf{C}_t = \mathbf{C}_{t-1} + \mathbf{X}_t^\top \mathbf{M}_t \mathbf{Y}_t. \quad (13)$$

The derivation is provided in Appendix F.

Finally, at task t , the incremental image classifier, $\hat{\mathbf{W}}_t$ is learned recursively for different classes using the feature \mathbf{X}_t , updated label $\tilde{\mathbf{Y}}_t$, the stored matrix \mathbf{A}_{t-1} , \mathbf{C}_{t-1} and weigh adjustment strategy.

3.6 INFERENCE STEP

During inference, following the strategy of RAIL (Xu et al., 2024), we compute the final prediction by taking a weighted sum of the zero-shot prediction logits and the learned classification head logits.

4 EXPERIMENTS

4.1 EXPERIMENTAL DETAILS

Datasets. Following prior works (Zhou et al., 2025a;b), we evaluate our method on six widely used benchmark datasets: FGVC Aircraft (Maji et al., 2013), StanfordCars (Krause et al., 2013), CIFAR100 (Krizhevsky et al., 2009), CUB200 (Wah et al., 2011), ObjectNet (Barbu et al., 2019), and UCF (Soomro et al., 2012). The classes in each dataset are split according to two class incremental learning protocols: (1) No base classes: all classes are evenly and disjointly split into 10 tasks. (2) With base classes: the first task includes half of the total classes as base classes, and the remaining classes are divided into 5 incremental tasks.

Evaluation Metrics. Following prior works (Zhou et al., 2025a), we report two metrics to evaluate the performance: A_B and \bar{A} . A_B represents the accuracy at the final task. \bar{A} represents average accuracy across all tasks, computed as $\bar{A} = \frac{1}{B} \sum_{b=1}^B A_b$.

Comparison Methods. We compare our method with existing CIL methods based on vision-language models, including non-exemplar-based methods: MoE-Adapters (Yu et al., 2024), RAPF (Huang et al., 2024), ENGINE (Zhou et al., 2025a), RAIL (Xu et al., 2024) and unimodal CIL baseline CODA-Prompt (Smith et al., 2023). ENGINE proposed a re-ranking method to boost performance. For fair comparison, we report the results before applying re-ranking. The zero-shot prediction of CLIP is utilized to generate the pseudo labels for comparison methods. Additionally, we report results for zero-shot CLIP (denoted as ZS-CLIP) and N2L trained with ground truth labels for each sample, serving as the upper bound in this setting (denoted as Label). All methods use the same LAION-400M pre-trained CLIP ViT-B/16 backbone and identical task splits. Additional experiments with OpenAI pre-trained CLIP ViT-B/16 and comparison with exemplar-based methods, PROOF (Zhou et al., 2025b) and CLAP4CLIP (Jha et al., 2024), are provided in Appendix C.

Implementation Details. For hyperparameters, the threshold θ for feature dimensionality reduction is set to 10, and pseudo-labels are updated over 3 iterations. The standard deviation σ to sample intra-class weights is set to 0.5. All results are averaged over three runs. Experiments are conducted using PyTorch on an NVIDIA RTX 4090 GPU.

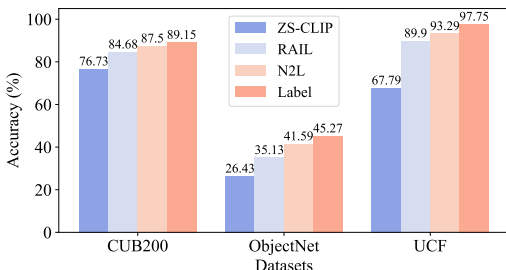


Figure 3: Comparison of ZS-CLIP, RAIL, N2L and, N2L with ground truth labels.

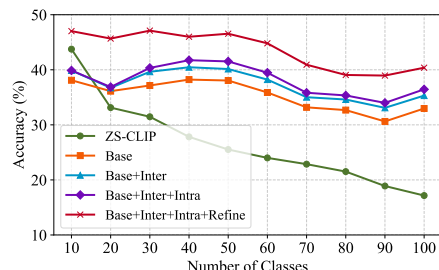


Figure 4: Ablation study of different components on Aircraft-B0Inc10.

4.2 MAIN RESULTS

Table. 1 summarizes the performance comparison across six datasets under various class-incremental settings. It can be observed that, the CIL methods designed for unimodel ViT achieve inferior performance, and even worse than the ZS-CLIP on some datasets such as Cars, CIFAR100 and CUB. This is because they only use the visual part of the CLIP, without utilizing the ability of aligning image and text in CLIP. The noisy pseudo label also hinders the learning of these methods and exacerbates forgetting. Our method consistently outperforms existing approaches in all scenarios. Notably, on datasets with large distribution shifts from CLIP’s pre-training data (e.g., Aircraft and ObjectNet), our method surpasses the second-best method by a significant margin of 2.75%-8.46%. For the remaining datasets, we also achieve consistent improvements of at least 2.82%, 0.46%, 1.77%, and 3.39% on Cars, CIFAR100, CUB, and UCF, respectively.

To further analyze the gap between learning without labels and learning with perfect labels, Fig. 3 and Table. 1 presents the results of ZS-CLIP, the second-best method RAIL, our method N2L, and an upper bound represented by N2L trained with ground truth labels. In addition to significantly outperforming both ZS-CLIP and RAIL, N2L narrows the gap to the upper bound by nearly 50% on Cars, ObjectNet and UCF, highlighting its effectiveness in incremental learning with unlabeled data.

In Table. 2, we compare our method with the unlabeled data learning approach CPL (Zhang et al., 2024). Specifically, we integrate CPL with various methods by replacing the pseudo labels with those produced by CPL. The results show that even when enhanced with CPL, existing methods still underperform compared to N2L. Furthermore, N2L itself achieves better performance when combined with CPL.

These improvements stem from our feature dimensionality reduction-based pseudo label refinement strategy, which further refines noisy labels. Additionally, the proposed inter-class and intra-class weight adjustment schemes help balance class frequency and leverage prediction confidence. Moreover, our regression-based learning objective with weight adjustment is inherently more robust to label noise than the traditional cross-entropy loss and can be solved in a recursive manner, thereby mitigating forgetting.

4.3 FURTHER ANALYSIS.

Effectiveness of Different Components. Fig. 4 presents an ablation study on different components of our approach. The baseline method is RAIL (Xu et al., 2024), which employs the ridge regression in Eq.2 to optimize the classifier. RAIL outperforms ZS-CLIP on most tasks, benefiting from its noise-robust regression objective and the recursively calculated classifier, which can be solved in a recursive manner.

Results show that incorporating inter-class adjustment improves performance, which can be attributed to its effectiveness in alleviating class frequency imbalance caused by imperfect pseudo labels. Moreover, the proposed intra-class adjustment strategy further enhances performance by assigning greater weight to high-confidence samples and reducing the influence of low-confidence ones, thereby minimizing the impact of erroneous pseudo labels. Finally, the proposed pseudo label refinement further leads to a dramatic performance gain on all tasks.

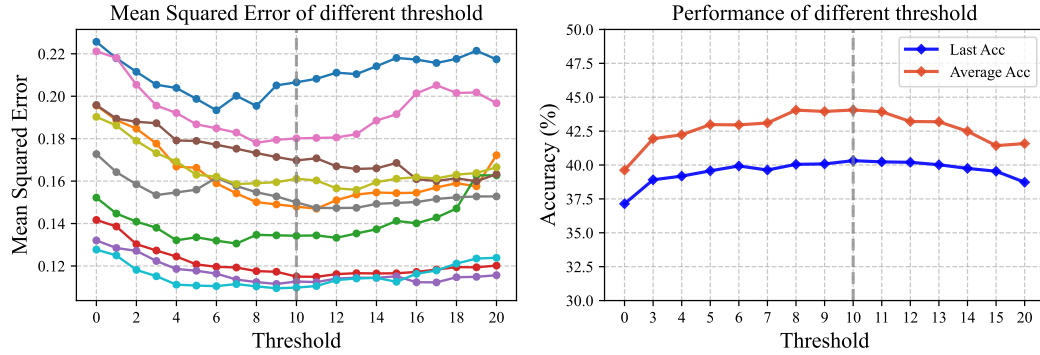


Figure 5: Left: MSE between the true labels and the predictions of classifiers learned on reduced features of different tasks across different thresholds. Different colors denote different tasks.
Right: the classification accuracy across different thresholds.

Table 2: Comparison of different methods combined with unlabeled learning method CPL.

Method	Aircraft-B0		CUB-B0	
	$\bar{\mathcal{A}}$	\mathcal{A}_B	$\bar{\mathcal{A}}$	\mathcal{A}_B
RAIL	36.23	33.59	81.64	73.93
RAIL + CPL	43.61	35.80	81.93	74.89
ENGINE	34.77	25.41	77.06	65.07
ENGINE + CPL	37.07	25.47	78.80	68.53
N2L	43.71	40.21	83.41	76.48
N2L + CPL	47.48	42.99	83.50	77.69

Table 3: Ablation of different intra-class adjustment methods on Aircraft-B0Inc10 setting.

Method	Aircraft-B0	
	$\bar{\mathcal{A}}$	\mathcal{A}_B
w/o. Intra-class Adjustment	43.39	39.69
w. Intra-class $\frac{1}{E}$	43.25	38.45
w. Intra-class $U(0.5, 1.5)$	<u>43.71</u>	40.08
w. Intra-class $U(0.25, 1.75)$	43.55	40.12
w. Intra-class $\mathcal{N}(1, \frac{1}{16})$	43.61	40.23
w. Intra-class $\mathcal{N}(1, \frac{1}{4})$	43.73	40.21

Progressive Label Refinement. The core of this component lies in the feature dimensionality reduction strategy, supported by the theoretical guarantee provided in Theorem 1. To evaluate whether removing certain singular directions of the feature matrix \mathbf{X} leads to lower mean squared error (MSE), we show the MSE between the true labels without noise and the predictions of classifiers learned on reduced features across different threshold values θ . Results for various tasks under the Aircraft-B0Inc10 setting are shown in the left of Fig. 5. The error curves exhibit a clear U-shape across tasks: as θ increases, more singular directions satisfying the inequality $\sigma^2 \geq (2\lambda + d_i^2)(\alpha_i^*)^2$ are removed, which leads to a drop in error. However, when θ becomes too large, even singular directions that do not meet this condition are eliminated, resulting in increased error. The corresponding accuracy curves for different θ values, shown on the right, follow a similar trend. We empirically set $\theta = 10$.

Bi-level Weight Adjustment. To evaluate inter-class adjustment, we visualize the norm of the classifier for different classes across tasks in the Aircraft-B0Inc10 setting in Fig. 6. The results demonstrate that the proposed inter-class adjustment strategy significantly suppresses large norms, preventing classes with more samples from dominating the classifier and thereby improving class balance. Table. 3 presents the performance of various intra-class adjustment strategies. The first row, which omits intra-class adjustment, yields the lowest performance, highlighting the necessity of incorporating such techniques. When intra-class adjustment is applied, using the reciprocal of entropy as the weighting factor results in lower performance compared to not applying weight adjustment. This is because it assigns excessively large weights to low entropy (high confidence) samples, which

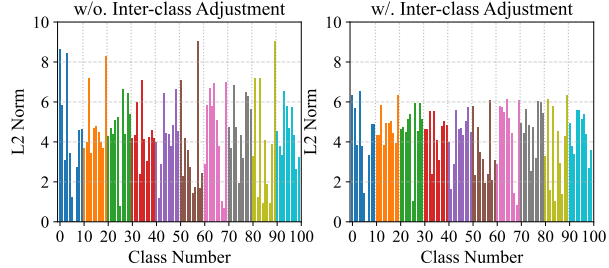


Figure 6: Norm of the classifier for different classes.

may dominate the learning and bias the model. Weight generation strategies that sample from predefined distributions, such as uniform and Gaussian, demonstrate improved performance. Among them, the Gaussian distribution $\mathcal{N}(1, \frac{1}{4})$ achieves better overall results on both $\bar{\mathcal{A}}$ and \mathcal{A}_B . Therefore, we adopt $\mathcal{N}(1, \frac{1}{4})$ for intra-class adjustment in our approach.

5 CONCLUSION

In this work, we introduce a more realistic paradigm for class incremental learning with vision-language model in which, at each task, only class names and unlabeled data for new categories are provided. To tackle this problem, we proposed N2L, a method that combines the regression learning objective with two key mechanisms. First, a pseudo label refinement method is proposed to iteratively refine initial pseudo labels by learning a label refinement classifier on features after dimensionality reduction, with theoretical guarantees on its denoising effectiveness. Second, we adopt a learning strategy comprising inter-class adjustment to address class imbalance introduced by pseudo labels, and intra-class adjustment to downweight low-confidence samples, thereby reducing the impact of noisy supervision. This regression with weight adjustment can be solved in a recursive form, achieving identical performance to joint training with unlabeled data and mitigating forgetting. Our work paves the way for more annotation-efficient incremental learning.

6 ACKNOWLEDGMENTS

This work was supported by the National Natural Science Foundation of China (62376011) and the National Key R&D Program of China (2024YFA1410000).

REFERENCES

- Rahaf Aljundi, Francesca Babiloni, Mohamed Elhoseiny, Marcus Rohrbach, and Tinne Tuytelaars. Memory aware synapses: Learning what (not) to forget. In *Proceedings of the European conference on computer vision (ECCV)*, pp. 139–154, 2018.
- Andrei Barbu, David Mayo, Julian Alverio, William Luo, Christopher Wang, Dan Gutfreund, Josh Tenenbaum, and Boris Katz. Objectnet: A large-scale bias-controlled dataset for pushing the limits of object recognition models. *Advances in neural information processing systems*, 32, 2019.
- Lukas Bossard, Matthieu Guillaumin, and Luc Van Gool. Food-101—mining discriminative components with random forests. In *Computer vision—ECCV 2014: 13th European conference, zurich, Switzerland, September 6–12, 2014, proceedings, part VI 13*, pp. 446–461. Springer, 2014.
- Alexey Dosovitskiy, Lucas Beyer, Alexander Kolesnikov, Dirk Weissenborn, Xiaohua Zhai, Thomas Unterthiner, Mostafa Dehghani, Matthias Minderer, Georg Heigold, Sylvain Gelly, Jakob Uszkoreit, and Neil Houlsby. An image is worth 16x16 words: Transformers for image recognition at scale. *ICLR*, 2021.
- Arthur Douillard, Alexandre Ramé, Guillaume Couairon, and Matthieu Cord. Dytox: Transformers for continual learning with dynamic token expansion. In *Proceedings of the IEEE/CVF conference on computer vision and pattern recognition*, pp. 9285–9295, 2022.
- Di Fang, Yinan Zhu, Runze Fang, Cen Chen, Ziqian Zeng, and Huiping Zhuang. Air: Analytic imbalance rectifier for continual learning. *arXiv preprint arXiv:2408.10349*, 2024.
- Robert M French. Catastrophic forgetting in connectionist networks. *Trends in cognitive sciences*, 3(4):128–135, 1999.
- Zijian Gao, Xingxing Zhang, Kele Xu, Xinjun Mao, and Huaimin Wang. Stabilizing zero-shot prediction: A novel antidote to forgetting in continual vision-language tasks. *Advances in Neural Information Processing Systems*, 37:128462–128488, 2024.
- Aritra Ghosh, Himanshu Kumar, and P Shanti Sastry. Robust loss functions under label noise for deep neural networks. In *Proceedings of the AAAI conference on artificial intelligence*, volume 31, 2017.
- Dan Hendrycks, Steven Basart, Norman Mu, Saurav Kadavath, Frank Wang, Evan Dorundo, Rahul Desai, Tyler Zhu, Samyak Parajuli, Mike Guo, et al. The many faces of robustness: A critical analysis of out-of-distribution generalization. In *Proceedings of the IEEE/CVF international conference on computer vision*, pp. 8340–8349, 2021.
- Zhiyuan Hu, Yunsheng Li, Jiancheng Lyu, Dashan Gao, and Nuno Vasconcelos. Dense network expansion for class incremental learning. In *Proceedings of the IEEE/CVF Conference on Computer Vision and Pattern Recognition*, pp. 11858–11867, 2023.
- Linlan Huang, Xusheng Cao, Haori Lu, and Xialei Liu. Class-incremental learning with clip: Adaptive representation adjustment and parameter fusion. In *European Conference on Computer Vision*, pp. 214–231. Springer, 2024.
- Tony Huang, Jack Chu, and Fangyun Wei. Unsupervised prompt learning for vision-language models. *arXiv preprint arXiv:2204.03649*, 2022.
- Saurav Jha, Dong Gong, and Lina Yao. Clap4clip: Continual learning with probabilistic finetuning for vision-language models. *arXiv preprint arXiv:2403.19137*, 2024.
- Minsoo Kang, Jaeyoo Park, and Bohyung Han. Class-incremental learning by knowledge distillation with adaptive feature consolidation. In *Proceedings of the IEEE/CVF conference on computer vision and pattern recognition*, pp. 16071–16080, 2022.
- James Kirkpatrick, Razvan Pascanu, Neil Rabinowitz, Joel Veness, Guillaume Desjardins, Andrei A Rusu, Kieran Milan, John Quan, Tiago Ramalho, Agnieszka Grabska-Barwinska, et al. Overcoming catastrophic forgetting in neural networks. *Proceedings of the national academy of sciences*, 114(13):3521–3526, 2017.

- Jonathan Krause, Michael Stark, Jia Deng, and Li Fei-Fei. 3d object representations for fine-grained categorization. In *Proceedings of the IEEE international conference on computer vision workshops*, pp. 554–561, 2013.
- Alex Krizhevsky, Geoffrey Hinton, et al. Learning multiple layers of features from tiny images. 2009.
- Dong-Hyun Lee et al. Pseudo-label: The simple and efficient semi-supervised learning method for deep neural networks. In *Workshop on challenges in representation learning, ICML*, volume 3, pp. 896. Atlanta, 2013.
- Qiwei Li and Jiahuan Zhou. Caprompt: Cyclic prompt aggregation for pre-trained model based class incremental learning. In *Proceedings of the AAAI Conference on Artificial Intelligence*, volume 39, pp. 18421–18429, 2025.
- Qiwei Li, Yuxin Peng, and Jiahuan Zhou. Fcs: Feature calibration and separation for non-exemplar class incremental learning. In *Proceedings of the IEEE/CVF conference on computer vision and pattern recognition*, pp. 28495–28504, 2024a.
- Qiwei Li, Yuxin Peng, and Jiahuan Zhou. Progressive prototype evolving for dual-forgetting mitigation in non-exemplar online continual learning. In *Proceedings of the 32nd ACM International Conference on Multimedia*, pp. 2477–2486, 2024b.
- Zhizhong Li and Derek Hoiem. Learning without forgetting. *IEEE transactions on pattern analysis and machine intelligence*, 40(12):2935–2947, 2017.
- Yan-Shuo Liang and Wu-Jun Li. Inflora: Interference-free low-rank adaptation for continual learning. In *Proceedings of the IEEE/CVF Conference on Computer Vision and Pattern Recognition*, pp. 23638–23647, 2024.
- Yaoyao Liu, Yuting Su, An-An Liu, Bernt Schiele, and Qianru Sun. Mnemonics training: Multi-class incremental learning without forgetting. In *Proceedings of the IEEE/CVF conference on Computer Vision and Pattern Recognition*, pp. 12245–12254, 2020.
- David Lopez-Paz and Marc’Aurelio Ranzato. Gradient episodic memory for continual learning. *Advances in neural information processing systems*, 30, 2017.
- Subhransu Maji, Esa Rahtu, Juho Kannala, Matthew Blaschko, and Andrea Vedaldi. Fine-grained visual classification of aircraft. *arXiv preprint arXiv:1306.5151*, 2013.
- Muhammad Jehanzeb Mirza, Leonid Karlinsky, Wei Lin, Horst Possegger, Mateusz Kozinski, Rogerio Feris, and Horst Bischof. Lafter: Label-free tuning of zero-shot classifier using language and unlabeled image collections. *Advances in Neural Information Processing Systems*, 36:5765–5777, 2023.
- Alec Radford, Jong Wook Kim, Chris Hallacy, Aditya Ramesh, Gabriel Goh, Sandhini Agarwal, Girish Sastry, Amanda Askell, Pamela Mishkin, Jack Clark, et al. Learning transferable visual models from natural language supervision. In *International conference on machine learning*, pp. 8748–8763. PmLR, 2021.
- Antti Rasmus, Mathias Berglund, Mikko Honkala, Harri Valpola, and Tapani Raiko. Semi-supervised learning with ladder networks. *Advances in neural information processing systems*, 28, 2015.
- James Seale Smith, Leonid Karlinsky, Vyshnavi Gutta, Paola Cascante-Bonilla, Donghyun Kim, Assaf Arbelle, Rameswar Panda, Rogerio Feris, and Zsolt Kira. Coda-prompt: Continual decomposed attention-based prompting for rehearsal-free continual learning. In *Proceedings of the IEEE/CVF conference on computer vision and pattern recognition*, pp. 11909–11919, 2023.
- Kihyuk Sohn, David Berthelot, Nicholas Carlini, Zizhao Zhang, Han Zhang, Colin A Raffel, Ekin Dogus Cubuk, Alexey Kurakin, and Chun-Liang Li. Fixmatch: Simplifying semi-supervised learning with consistency and confidence. *Advances in neural information processing systems*, 33:596–608, 2020.
- Khurram Soomro, Amir Roshan Zamir, and Mubarak Shah. Ucf101: A dataset of 101 human actions classes from videos in the wild. *arXiv preprint arXiv:1212.0402*, 2012.

- Zhicheng Sun, Yadong Mu, and Gang Hua. Regularizing second-order influences for continual learning. In *Proceedings of the IEEE/CVF Conference on Computer Vision and Pattern Recognition*, pp. 20166–20175, 2023.
- Yuwen Tan, Qinhao Zhou, Xiang Xiang, Ke Wang, Yuchuan Wu, and Yongbin Li. Semantically-shifted incremental adapter-tuning is a continual vitrtransformer. In *Proceedings of the IEEE/CVF Conference on Computer Vision and Pattern Recognition*, pp. 23252–23262, 2024.
- Marco Toldo and Mete Ozay. Bring evanescent representations to life in lifelong class incremental learning. In *Proceedings of the IEEE/CVF Conference on Computer Vision and Pattern Recognition*, pp. 16732–16741, 2022.
- Catherine Wah, Steve Branson, Peter Welinder, Pietro Perona, and Serge Belongie. The caltech-ucsd birds-200-2011 dataset. 2011.
- Fu-Yun Wang, Da-Wei Zhou, Liu Liu, Han-Jia Ye, Yatao Bian, De-Chuan Zhan, and Peilin Zhao. Beef: Bi-compatible class-incremental learning via energy-based expansion and fusion. In *The eleventh international conference on learning representations*, 2022a.
- Liyuan Wang, Jingyi Xie, Xingxing Zhang, Mingyi Huang, Hang Su, and Jun Zhu. Hierarchical decomposition of prompt-based continual learning: Rethinking obscured sub-optimality. *Advances in Neural Information Processing Systems*, 36:69054–69076, 2023.
- Liyuan Wang, Xingxing Zhang, Hang Su, and Jun Zhu. A comprehensive survey of continual learning: Theory, method and application. *IEEE Transactions on Pattern Analysis and Machine Intelligence*, 2024.
- Zifeng Wang, Zizhao Zhang, Sayna Ebrahimi, Ruoxi Sun, Han Zhang, Chen-Yu Lee, Xiaoqi Ren, Guolong Su, Vincent Perot, Jennifer Dy, et al. Dualprompt: Complementary prompting for rehearsal-free continual learning. In *European conference on computer vision*, pp. 631–648. Springer, 2022b.
- Zifeng Wang, Zizhao Zhang, Chen-Yu Lee, Han Zhang, Ruoxi Sun, Xiaoqi Ren, Guolong Su, Vincent Perot, Jennifer Dy, and Tomas Pfister. Learning to prompt for continual learning. In *Proceedings of the IEEE/CVF conference on computer vision and pattern recognition*, pp. 139–149, 2022c.
- Yichen Wu, Hongming Piao, Long-Kai Huang, Renzhen Wang, Wanhua Li, Hanspeter Pfister, Deyu Meng, Kede Ma, and Ying Wei. Sd-lora: Scalable decoupled low-rank adaptation for class incremental learning. In *The Thirteenth International Conference on Learning Representations*, 2025.
- Jianxiong Xiao, James Hays, Krista A Ehinger, Aude Oliva, and Antonio Torralba. Sun database: Large-scale scene recognition from abbey to zoo. In *2010 IEEE computer society conference on computer vision and pattern recognition*, pp. 3485–3492. IEEE, 2010.
- Yicheng Xu, Yuxin Chen, Jiahao Nie, Yusong Wang, Huiping Zhuang, and Manabu Okumura. Advancing cross-domain discriminability in continual learning of vision-language models. *arXiv preprint arXiv:2406.18868*, 2024.
- Jiazu Yu, Yunzhi Zhuge, Lu Zhang, Ping Hu, Dong Wang, Huchuan Lu, and You He. Boosting continual learning of vision-language models via mixture-of-experts adapters. In *Proceedings of the IEEE/CVF Conference on Computer Vision and Pattern Recognition*, pp. 23219–23230, 2024.
- Jiahan Zhang, Qi Wei, Feng Liu, and Lei Feng. Candidate pseudolabel learning: Enhancing vision-language models by prompt tuning with unlabeled data. *arXiv preprint arXiv:2406.10502*, 2024.
- Junting Zhang, Jie Zhang, Shalini Ghosh, Dawei Li, Serafettin Tasçi, Larry Heck, Heming Zhang, and C-C Jay Kuo. Class-incremental learning via deep model consolidation. In *Proceedings of the IEEE/CVF winter conference on applications of computer vision*, pp. 1131–1140, 2020.
- Mengyu Zheng, Yehui Tang, Zhiwei Hao, Kai Han, Yunhe Wang, and Chang Xu. Adapt without forgetting: Distill proximity from dual teachers in vision-language models. In *European Conference on Computer Vision*, pp. 109–125. Springer, 2024.

- Zangwei Zheng, Mingyuan Ma, Kai Wang, Ziheng Qin, Xiangyu Yue, and Yang You. Preventing zero-shot transfer degradation in continual learning of vision-language models. In *Proceedings of the IEEE/CVF international conference on computer vision*, pp. 19125–19136, 2023.
- Da-Wei Zhou, Hai-Long Sun, Jingyi Ning, Han-Jia Ye, and De-Chuan Zhan. Continual learning with pre-trained models: a survey. In *Proceedings of the Thirty-Third International Joint Conference on Artificial Intelligence*, pp. 8363–8371, 2024a.
- Da-Wei Zhou, Hai-Long Sun, Han-Jia Ye, and De-Chuan Zhan. Expandable subspace ensemble for pre-trained model-based class-incremental learning. In *Proceedings of the IEEE/CVF Conference on Computer Vision and Pattern Recognition*, pp. 23554–23564, 2024b.
- Da-Wei Zhou, Qi-Wei Wang, Zhi-Hong Qi, Han-Jia Ye, De-Chuan Zhan, and Ziwei Liu. Class-incremental learning: A survey. *IEEE Transactions on Pattern Analysis and Machine Intelligence*, 2024c.
- Da-Wei Zhou, Kai-Wen Li, Jingyi Ning, Han-Jia Ye, Lijun Zhang, and De-Chuan Zhan. External knowledge injection for clip-based class-incremental learning. *arXiv preprint arXiv:2503.08510*, 2025a.
- Da-Wei Zhou, Yuanhan Zhang, Yan Wang, Jingyi Ning, Han-Jia Ye, De-Chuan Zhan, and Ziwei Liu. Learning without forgetting for vision-language models. *IEEE Transactions on Pattern Analysis and Machine Intelligence*, 2025b.
- Fei Zhu, Xu-Yao Zhang, Chuang Wang, Fei Yin, and Cheng-Lin Liu. Prototype augmentation and self-supervision for incremental learning. In *Proceedings of the IEEE/CVF conference on computer vision and pattern recognition*, pp. 5871–5880, 2021.
- Huiping Zhuang, Zhenyu Weng, Hongxin Wei, RENCHUNZI Xie, Kar-Ann Toh, and Zhiping Lin. Acil: Analytic class-incremental learning with absolute memorization and privacy protection. *Advances in Neural Information Processing Systems*, 35:11602–11614, 2022.
- Huiping Zhuang, Yizhu Chen, Di Fang, Run He, Kai Tong, Hongxin Wei, Ziqian Zeng, and Cen Chen. Gacl: Exemplar-free generalized analytic continual learning. *Advances in Neural Information Processing Systems*, 37:83024–83047, 2024.

A LIMITATION

In this paper, we propose a setting where only unlabeled data and class names are provided for each incremental task. We assume that the unlabeled data strictly corresponds to the given class names. However, in real-world scenarios, this assumption may not hold, the collected data could include samples from previously seen classes as well as from unseen future classes not included in either the current or past tasks. As part of future work, we plan to explore a more challenging setting where the unlabeled data may contain a mix of past, present, and future classes.

B CODE

We provide the core implementation of the training process in `code.py`. The `incremental_train()` function serves as the main entry point for performing incremental training, while the `train()` function carries out the training for each incremental task.

C MORE RESULTS

C.1 DIFFERENT EPOCHS OF PROGRESSIVE LABEL REFINEMENT

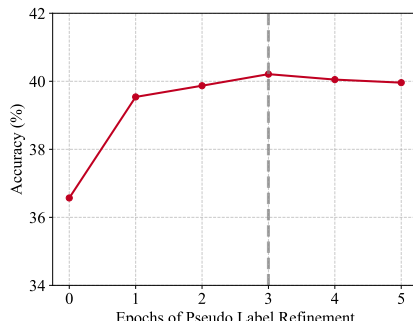


Figure 7: Results on Aircraft B0Inc10 with different epochs of progressive label refinement.

In Fig. 7, we present an ablation study on the number of epochs used for label refinement. Setting the number of epochs to 0, meaning the pseudo label refinement strategy is not applied, results in the lowest performance. When the refinement strategy is incorporated, there is a significant improvement in performance. Moreover, the results remain stable when the number of epochs is set between 2 and 5. Based on these observations, we choose 3 epochs as the default setting in our experiments.

C.2 COMPARISON WITH EXEMPLAR-BASED METHODS

In Table 4, we compare our method with existing exemplar-based approaches, PROOF (Zhou et al., 2025b) and CLAP4CLIP (Jha et al., 2024). Following their setting, the exemplar buffer uses a fixed memory strategy that stores 20 samples per class. In contrast, our method does not use any exemplars, i.e., the exemplar buffer size is zero. Results show that even without storing exemplars, N2L outperforms existing methods on all datasets, except for the setting with base classes on CIFAR100, CUB, and ObjectNet, where the performance gap is only 0.27%, 0.58%, and 0.43% respectively. These results highlight N2L’s strong ability to mitigate forgetting, primarily due to the recursively computed closed-form solution for the classification head, along with intra-class and inter-class adjustment strategies. Additionally, the proposed pseudo-label refinement method contributes to more accurate label refinement.

Table 4: Comparison with exemplar-based methods. Best scores are in **bold**. The second-best scores are in underline.

Method	Aircraft				Cars				CIFAR100			
	B0Inc10		B50Inc10		B0Inc10		B50Inc10		B0Inc10		B50Inc10	
	\bar{A}	\mathcal{A}_B										
ZS-CLIP	26.61	17.16	21.66	17.16	82.90	76.73	78.74	76.73	81.81	71.38	76.49	71.38
CLAP4CLIP	<u>41.15</u>	<u>35.81</u>	26.88	<u>28.43</u>	<u>90.02</u>	<u>86.46</u>	79.68	75.88	<u>86.34</u>	<u>79.11</u>	<u>82.90</u>	80.57
PROOF	38.10	33.62	<u>28.10</u>	28.15	89.23	85.09	<u>83.83</u>	<u>83.03</u>	84.85	77.47	79.17	76.36
N2L	43.73	40.21	29.69	32.42	92.38	87.50	86.42	85.45	87.80	81.13	82.92	<u>80.30</u>
CUB												
Method	ObjectNet				UCF							
	B0Inc20		B100Inc20		B0Inc20		B100Inc20		B0Inc10		B50Inc10	
	\bar{A}	\mathcal{A}_B										
ZS-CLIP	75.47	63.72	69.06	63.72	38.43	26.43	31.12	26.43	75.88	67.79	71.68	67.79
CLAP4CLIP	<u>82.45</u>	<u>74.85</u>	75.74	<u>72.71</u>	<u>49.00</u>	<u>38.55</u>	41.85	<u>37.77</u>	87.10	83.82	<u>81.38</u>	<u>83.50</u>
PROOF	80.50	73.98	73.74	71.83	45.46	34.93	35.36	32.16	<u>89.41</u>	<u>86.00</u>	81.23	81.76
N2L	83.41	76.48	<u>75.16</u>	73.40	49.31	41.59	41.42	38.65	95.00	93.29	86.41	87.87

Table 5: Comparison of different methods with OpenAI pre-trained weight. Best scores are in **bold**. The second-best scores are in underline.

Method	Aircraft				Cars				CIFAR100			
	B0Inc10		B50Inc10		B0Inc10		B50Inc10		B0Inc10		B50Inc10	
	\bar{A}	\mathcal{A}_B										
ZS-CLIP	32.96	21.96	27.40	21.96	71.99	56.36	64.51	56.36	78.66	68.22	72.97	68.22
Label	64.11	53.42	<u>57.04</u>	53.45	87.79	79.22	83.60	79.23	87.23	79.94	82.40	79.98
CODA-Prompt	32.59	22.89	22.30	15.75	68.91	53.34	54.89	43.56	77.94	64.98	64.21	52.00
MoE-Adapter	33.37	22.87	27.75	22.55	70.64	56.39	63.43	55.88	80.17	69.69	74.44	69.86
RAPF	36.10	25.68	26.57	23.63	73.36	57.02	61.55	55.10	83.43	74.84	76.08	73.26
RAIL	<u>42.44</u>	<u>37.72</u>	27.86	<u>28.77</u>	<u>80.33</u>	<u>69.55</u>	66.96	<u>63.88</u>	<u>85.59</u>	<u>77.78</u>	<u>77.81</u>	<u>75.82</u>
ENGINE	38.40	27.97	<u>30.30</u>	25.45	76.72	62.14	<u>69.38</u>	62.42	82.94	73.29	77.03	72.85
N2L	46.75	42.11	30.46	32.88	83.65	75.47	74.32	71.94	86.35	79.00	79.38	78.03
CUB												
Method	ObjectNet				UCF							
	B0Inc20		B100Inc20		B0Inc20		B100Inc20		B0Inc10		B50Inc10	
	\bar{A}	\mathcal{A}_B										
ZS-CLIP	68.48	54.04	59.95	54.04	45.61	33.01	38.16	33.01	79.92	70.75	76.22	70.75
Label	84.55	76.45	79.92	76.46	57.81	47.93	52.99	47.90	98.73	97.32	98.26	97.32
CODA-Prompt	64.40	46.89	47.75	35.09	42.45	30.11	31.24	23.43	82.23	74.84	68.27	58.96
MoE-Adapter	67.93	54.44	59.37	54.52	44.83	33.46	38.24	33.79	80.09	71.66	74.96	70.62
RAPF	69.33	51.58	56.96	48.94	48.91	34.92	38.83	33.63	89.10	83.11	79.37	76.51
RAIL	<u>78.57</u>	<u>70.01</u>	<u>66.58</u>	<u>65.01</u>	48.37	<u>41.22</u>	39.08	<u>36.59</u>	<u>91.86</u>	<u>90.70</u>	82.93	<u>84.96</u>
ENGINE	72.80	58.29	64.34	58.32	<u>50.00</u>	35.58	40.49	34.53	90.02	85.73	<u>84.76</u>	82.85
N2L	81.18	72.58	69.99	68.01	54.99	45.21	45.26	42.09	95.58	93.57	89.16	89.91

C.3 DIFFERENT PRE-TRAINED WEIGHTS

In the main paper, we compare various methods using the CLIP model pre-trained on LAION400M¹. In Table 5, we present the results using the CLIP model pre-trained by OpenAI². The results demonstrate that N2L consistently outperforms other methods across both settings.

¹https://github.com/mlfoundations/open_clip

²<https://github.com/openai/CLIP>

Table 6: Comparison of different methods on Food, ImageNet-R, and SUN datasets.

Method	Food				ImageNet-R				SUN			
	B0Inc10		B50Inc10		B0Inc20		B100Inc20		B0Inc30		B150Inc30	
	$\bar{\mathcal{A}}$	\mathcal{A}_B										
ZS-CLIP	87.86	81.99	84.78	81.99	83.12	76.62	79.23	76.62	79.45	72.14	74.99	72.14
ENGINE	88.30	81.78	84.72	81.55	84.14	76.93	79.26	76.56	83.04	76.17	78.06	75.10
ENGINE + Label	88.52	81.85	85.08	81.59	84.61	77.12	79.96	76.78	83.51	76.21	78.83	75.20
N2L	90.58	85.50	87.18	85.01	86.00	81.06	81.89	80.29	84.38	78.85	79.15	77.40
N2L + Label	90.95	85.84	88.38	85.84	86.61	81.52	83.88	81.51	87.42	81.50	84.31	81.50

C.4 MORE DATASETS

Following the setting of ENGINE (Zhou et al., 2025a), in Table 6, we also report the results of three datasets: Food (Bossard et al., 2014), ImageNet-R (Hendrycks et al., 2021), and SUN (Xiao et al., 2010). ENGINE + Label and N2L + Label represent providing the methods with annotated data instead of unlabeled data in ENGINE and N2L. In these datasets, results show that the gap between learning with unlabeled data and annotated data is small. This is because these datasets have a high zero-shot performance, making the generated pseudo labels more reliable, which aids the learning with unlabeled data. On these datasets, N2L with unlabeled data even achieves comparable performance to the ENGINE + Label.

D INTRODUCTION ABOUT COMPARISON METHODS

ZS-CLIP. This method enables direct inference without requiring training on specific downstream tasks. It leverages the pretrained image-text alignment ability of CLIP to recognize images.

CODA-Prompt (Smith et al., 2023). This method introduces an attention-based end-to-end key-query framework. It learns a set of prompt components and combines them using input-conditioned attention weights to generate input-aware prompts, thereby enhancing the model’s adaptability to new tasks. This method relies solely on the visual branch of CLIP.

MoE-Adapters (Yu et al., 2024). This method adapts to continuously arriving tasks by dynamically inserting Mixture-of-Experts adapters into a pre-trained CLIP model. It enables progressive model expansion without altering the original backbone, effectively mitigating forgetting in long-term continual learning.

RAPF (Huang et al., 2024). This method is built upon a frozen pre-trained CLIP. During the training of new tasks, it measures the influence of new classes on old ones using textual features and adaptively adjusts the representations of old classes. In the adapter fine-tuning phase, a decomposed parameter fusion strategy is introduced to further mitigate forgetting.

RAIL (Xu et al., 2024). This method employs a recursive ridge regression-based adapter to learn tasks across multiple domains and decouples inter-domain correlations by projecting features into a higher-dimensional space. It also uses a training-free fusion module to preserve zero-shot capability without the need for reference data.

ENGINE (Zhou et al., 2025a). This method employs a dual-branch tuning framework: the visual branch enriches image features through data augmentation, the textual branch leverages GPT-4 to generate more discriminative class descriptions, and during inference, a re-ranking strategy is applied to further improve prediction results.

The following are two exemplar-based methods. For a fair comparison, we adopt a storage strategy of 20 samples per class for both methods.

CLAP4CLIP (Jha et al., 2024). This method performs probabilistic modeling over the visual-guided textual features for each task, enabling a more reliable continual learning fine-tuning strategy. Unlike traditional forgetting-mitigation methods that rely on large amounts of data, it leverages the rich prior knowledge of CLIP for parameter initialization and distribution regularization.

PROOF (Zhou et al., 2025b). This method trains task-specific projection modules for each task, expands new projections while keeping the old ones fixed, and introduces a fusion module to jointly adjust visual and textual features.

E DETAILS OF THEOREM 1

E.1 PROOF OF THEOREM 1

Theorem 1. Consider the regression model with noisy labels: $\mathbf{y} = \mathbf{X}\mathbf{w}^* + \boldsymbol{\varepsilon}$, where features are $\mathbf{X} \in \mathbb{R}^{n \times d}$, $\mathbf{w}^* \in \mathbb{R}^d$ is the true regression coefficient vector, and $\boldsymbol{\varepsilon}$ is the noise with zero mean and variance σ^2 . Let the SVD of $\mathbf{X} = \mathbf{U}\mathbf{D}\mathbf{V}^\top$, $\mathbf{V} = [\mathbf{v}_1, \dots, \mathbf{v}_d]$. α_i is the i -th coordinate of vector $\boldsymbol{\alpha}^* = \mathbf{V}^\top \mathbf{w}^*$.

If $\sigma^2 \geq (2\lambda + d_j^2)(\alpha_j^*)^2$, projecting \mathbf{X} onto the eigenvectors without j -th components (denoted $\mathbf{X}' = \mathbf{U}\mathbf{D}\mathbf{V}^\top \mathbf{V}'$) yields a smaller expected mean squared error:

$$\mathbb{E} [\|\mathbf{X}'\hat{\mathbf{w}}' - \mathbf{X}\mathbf{w}^*\|_F^2] \leq \mathbb{E} [\|\mathbf{X}\hat{\mathbf{w}} - \mathbf{X}\mathbf{w}^*\|_F^2], \quad (14)$$

where $\hat{\mathbf{w}}$ and $\hat{\mathbf{w}}'$ are the regression solutions using \mathbf{X} and \mathbf{X}' , $\mathbf{V}' = [\mathbf{v}_1, \dots, \mathbf{v}_{j-1}, \mathbf{v}_{j+1}, \dots, \mathbf{v}_d]$.

Proof.

The objective function of Ridge Regression is given by:

$$\min_{\mathbf{w}} \|\mathbf{y} - \mathbf{X}\mathbf{w}\|_F^2 + \lambda \|\mathbf{w}\|_F^2, \quad (15)$$

whose analytical solution is:

$$\hat{\mathbf{w}} = (\mathbf{X}^\top \mathbf{X} + \lambda \mathbf{I})^{-1} \mathbf{X}^\top \mathbf{y}. \quad (16)$$

Substituting the SVD into the ridge solution, we get:

$$\begin{aligned} \hat{\mathbf{w}} &= (\mathbf{X}^\top \mathbf{X} + \lambda \mathbf{I})^{-1} \mathbf{X}^\top \mathbf{y} \\ &= (\mathbf{V}\mathbf{D}^2 \mathbf{V}^\top + \lambda \mathbf{I})^{-1} \mathbf{V}\mathbf{D}\mathbf{U}^\top \mathbf{y}. \\ &= \mathbf{V}(\mathbf{D}^2 + \lambda \mathbf{I})^{-1} \mathbf{D}\mathbf{U}^\top \mathbf{y}. \end{aligned} \quad (17)$$

According to the definition $\boldsymbol{\alpha}^* = \mathbf{V}^\top \mathbf{w}^* = (\alpha_1^*, \alpha_2^*, \dots)^\top$, we have $\mathbf{X}\mathbf{w}^* = \mathbf{U}\mathbf{D}\boldsymbol{\alpha}^*$.

Let $\hat{\boldsymbol{\alpha}} = (\mathbf{D}^2 + \lambda \mathbf{I})^{-1} \mathbf{D}\mathbf{U}^\top \mathbf{y}$, then according to Eq. 17, $\mathbf{X}\hat{\mathbf{w}} = \mathbf{U}\mathbf{D}\hat{\boldsymbol{\alpha}}$.

The mean squared error of the prediction is:

$$\begin{aligned} \text{MSE} &= \mathbb{E} [\|\mathbf{X}\hat{\mathbf{w}} - \mathbf{X}\mathbf{w}^*\|_F^2] \\ &= \mathbb{E} [\|\mathbf{U}\mathbf{D}(\hat{\boldsymbol{\alpha}} - \boldsymbol{\alpha}^*)\|_F^2] \\ &= \mathbb{E} [\|\mathbf{D}(\hat{\boldsymbol{\alpha}} - \boldsymbol{\alpha}^*)\|_F^2] \\ &= \sum_{i=1}^d d_i^2 \mathbb{E} [(\hat{\alpha}_i - \alpha_i^*)^2] \\ &= \sum_{i=1}^d d_i^2 \underbrace{(\mathbb{E}[\hat{\alpha}_i] - \alpha_i^*)^2}_{\text{Bias}_i^2} + \underbrace{d_i^2 \text{Var}(\hat{\alpha}_i)}_{\text{Var}_i}. \end{aligned} \quad (18)$$

The $\hat{\boldsymbol{\alpha}}$ can also be represented as:

$$\begin{aligned} \hat{\boldsymbol{\alpha}} &= (\mathbf{D}^2 + \lambda \mathbf{I})^{-1} \mathbf{D}\mathbf{U}^\top \mathbf{y} \\ &= (\mathbf{D}^2 + \lambda \mathbf{I})^{-1} \mathbf{D}\mathbf{U}^\top (\mathbf{X}\mathbf{w}^* + \boldsymbol{\varepsilon}) \\ &= (\mathbf{D}^2 + \lambda \mathbf{I})^{-1} \mathbf{D}\mathbf{U}^\top (\mathbf{U}\mathbf{D}\boldsymbol{\alpha}^* + \boldsymbol{\varepsilon}) \\ &= (\mathbf{D}^2 + \lambda \mathbf{I})^{-1} \mathbf{D}(\mathbf{D}\boldsymbol{\alpha}^* + \mathbf{U}^\top \boldsymbol{\varepsilon}), \end{aligned} \quad (19)$$

which can be decomposed into signal and noise components:

$$\hat{\alpha}_i = \frac{d_i^2}{d_i^2 + \lambda} \alpha_i^* + \frac{d_i}{d_i^2 + \lambda} (\mathbf{u}_i^\top \boldsymbol{\varepsilon}), \quad i = 1, \dots, d. \quad (20)$$

Bias: The expectation of the $\hat{\alpha}_i$:

$$\begin{aligned} \text{Bias}_i &= \mathbb{E}[\hat{\alpha}_i] - \alpha_i^* \\ &= \frac{d_i^2}{d_i^2 + \lambda} \alpha_i^* + \frac{d_i}{d_i^2 + \lambda} \mathbb{E}[\mathbf{u}_i^\top \boldsymbol{\varepsilon}] - \alpha_i^* \\ &= \left(\frac{d_i^2}{d_i^2 + \lambda} - 1 \right) \alpha_i^* \\ &= -\frac{\lambda}{d_i^2 + \lambda} \alpha_i^*. \end{aligned} \quad (21)$$

And the squared bias is:

$$\text{Bias}_i^2 = \left(\frac{\lambda}{d_i^2 + \lambda} \right)^2 (\alpha_i^*)^2. \quad (22)$$

Variance: The variance of $\hat{\alpha}_i$:

$$\begin{aligned} \text{Var}(\hat{\alpha}_i) &= \text{Var} \left(\frac{d_i^2}{d_i^2 + \lambda} \alpha_i^* + \frac{d_i}{d_i^2 + \lambda} \mathbf{u}_i^\top \boldsymbol{\varepsilon} \right) \\ &= \text{Var} \left(\frac{d_i}{d_i^2 + \lambda} \mathbf{u}_i^\top \boldsymbol{\varepsilon} \right) \\ &= \frac{d_i^2}{(d_i^2 + \lambda)^2} \sigma^2. \end{aligned} \quad (23)$$

Then the mean squared error is:

$$\begin{aligned} \text{MSE} &= \sum_{i=1}^d d_i^2 \left[(\mathbb{E}[\hat{\alpha}_i] - \alpha_i^*)^2 + \text{Var}(\hat{\alpha}_i) \right] \\ &= \sum_{i=1}^d d_i^2 \left[\left(\frac{\lambda}{d_i^2 + \lambda} \right)^2 (\alpha_i^*)^2 + \frac{d_i^2}{(d_i^2 + \lambda)^2} \sigma^2 \right] \\ &= \sum_{i=1}^d \frac{(\lambda d_i)^2}{(d_i^2 + \lambda)^2} (\alpha_i^*)^2 + \sum_{i=1}^d \frac{d_i^4}{(d_i^2 + \lambda)^2} \sigma^2. \end{aligned} \quad (24)$$

Consider removing the j -th singular direction:

$$\begin{aligned} \mathbf{X}' &= \mathbf{X}\mathbf{V}' \\ &= \mathbf{U}\mathbf{D}\mathbf{V}^\top \mathbf{V}' \\ &= [d_1 \mathbf{u}_1, \dots, d_{i-1} \mathbf{u}_{i-1}, d_{i+1} \mathbf{u}_{i+1}, \dots, d_n \mathbf{u}_n] \\ &= \mathbf{U}' \mathbf{D}' \end{aligned} \quad (25)$$

where \mathbf{U}' is removing j -th column of \mathbf{U} , and \mathbf{D}' is removing j -th column and row of \mathbf{D} .

The objective function of Ridge Regression is:

$$\min_{\mathbf{w}} \|\mathbf{y} - \mathbf{X}' \mathbf{w}\|_F^2 + \lambda \|\mathbf{w}\|_F^2, \quad (26)$$

whose analytical solution is:

$$\begin{aligned} \hat{\mathbf{w}}' &= (\mathbf{X}'^\top \mathbf{X}' + \lambda \mathbf{I})^{-1} \mathbf{X}'^\top \mathbf{y}. \\ &= (\mathbf{D}'^2 + \lambda \mathbf{I})^{-1} \mathbf{D}' \mathbf{U}'^\top \mathbf{y}. \end{aligned} \quad (27)$$

Similar to the definition of $\hat{\alpha}$, we also define $\hat{\alpha}'_j = (\mathbf{D}'^2 + \lambda \mathbf{I})^{-1} \mathbf{D}' \mathbf{U}'^\top \mathbf{y}$ then we have:

$$\begin{aligned}\hat{\alpha}' &= \hat{\mathbf{w}}' = (\mathbf{D}'^2 + \lambda \mathbf{I})^{-1} \mathbf{D}' \mathbf{U}'^\top \mathbf{y} \\ &= (\mathbf{D}'^2 + \lambda \mathbf{I})^{-1} \mathbf{D}' (\mathbf{D}' \boldsymbol{\alpha}^* + \mathbf{U}'^\top \boldsymbol{\varepsilon}),\end{aligned}\quad (28)$$

where

$$\hat{\alpha}'_i = \begin{cases} \frac{d_i^2}{d_i^2 + \lambda} \alpha_i^* + \frac{d_i}{d_i^2 + \lambda} (\mathbf{u}_i^\top \boldsymbol{\varepsilon}) = \hat{\alpha}_i, & i = 1, \dots, j-1 \\ \frac{d_{i+1}^2}{d_{i+1}^2 + \lambda} \alpha_{i+1}^* + \frac{d_{i+1}}{d_{i+1}^2 + \lambda} (\mathbf{u}_{i+1}^\top \boldsymbol{\varepsilon}) = \hat{\alpha}_{i+1}, & i = j, \dots, d-1 \end{cases} \quad (29)$$

$$(30)$$

Then the prediction error of using X_k is:

$$\begin{aligned}\text{MSE}' &= \mathbb{E} [\|\mathbf{X}' \hat{\mathbf{w}}' - \mathbf{X} \mathbf{w}^*\|_F^2] \\ &= \mathbb{E} [\|\mathbf{U}' \mathbf{D}' \hat{\alpha}' - \mathbf{U} \mathbf{D} \boldsymbol{\alpha}^*\|_F^2] \\ &= \sum_{i=1}^{j-1} d_i^2 \mathbb{E} [(\hat{\alpha}'_i - \alpha_i^*)^2] + \sum_{i=j}^{d-1} d_i^2 \mathbb{E} [(\hat{\alpha}'_i - \alpha_{i+1}^*)^2] + d_j^2 \mathbb{E} [(\alpha_j^*)^2] \\ &= \sum_{i=1}^{j-1} d_i^2 \mathbb{E} [(\hat{\alpha}_i - \alpha_i^*)^2] + \sum_{i=j+1}^d d_i^2 \mathbb{E} [(\hat{\alpha}_i - \alpha_i^*)^2] + d_j^2 \mathbb{E} [(\alpha_j^*)^2] \\ &= \text{MSE} - \mathbb{E} [(\hat{\alpha}_j - \alpha_j^*)^2] + d_j^2 \mathbb{E} [(\alpha_j^*)^2] \\ &= \text{MSE} - d_j^2 \left[(\mathbb{E}[\hat{\alpha}_j] - \alpha_j^*)^2 + \text{Var}(\hat{\alpha}_j) \right] + d_j^2 \mathbb{E} [(\alpha_j^*)^2] \\ &= \text{MSE} - \frac{(\lambda d_j)^2}{(d_j^2 + \lambda)^2} (\alpha_j^*)^2 - \frac{d_j^4}{(d_j^2 + \lambda)^2} \sigma^2 + d_j^2 (\alpha_j^*)^2.\end{aligned}\quad (31)$$

With the assumption that $\sigma^2 \geq (2\lambda + d_j^2)(\alpha_j^*)^2$:

$$\begin{aligned}d_j^2 (\alpha_j^*)^2 &= \frac{(\lambda d_j)^2}{(d_j^2 + \lambda)^2} (\alpha_j^*)^2 + d_j^2 \left(1 - \frac{\lambda^2}{(d_j^2 + \lambda)^2}\right) (\alpha_j^*)^2 \\ &= \frac{(\lambda d_j)^2}{(d_j^2 + \lambda)^2} (\alpha_j^*)^2 + d_j^4 \frac{(d_j^2 + 2\lambda)(\alpha_j^*)^2}{(d_j^2 + \lambda)^2} \\ &\leq \frac{(\lambda d_j)^2}{(d_j^2 + \lambda)^2} (\alpha_j^*)^2 + \frac{d_j^4}{(d_j^2 + \lambda)^2} \sigma^2.\end{aligned}\quad (32)$$

Then

$$\text{MSE}' \leq \text{MSE}, \quad (33)$$

finish the proof.

E.2 THE SCALE OF σ AND $\boldsymbol{\alpha}^*$

In this section, we show the scale of σ and $\boldsymbol{\alpha}^*$ to show that the assumption of $\sigma^2 \geq (2\lambda + d_j^2)(\alpha_j^*)^2$ in Theorem 1 can be achieved with appropriate d_j . λ is the regularization parameter of ridge regression which is typically 0.1. During the learning of task t , for a specific class k and the sample x_i , the ground truth label is a one-hot value $y_{i,k}$, the pseudo label is also a one-hot value $\tilde{y}_{i,k}$. Then the standard variance σ of class k can be estimated by $y_{i,k} - \tilde{y}_{i,k}$ with different samples. For $\boldsymbol{\alpha}^* = \mathbf{V}^\top \mathbf{w}^*$, \mathbf{V} is the part of the SVD decomposition of \mathbf{X} and \mathbf{w}^* can be estimated by solving ridge regression with the feature \mathbf{X} and ground truth label \mathbf{Y} . Then, we show the standard variance σ of different classes and the value of different dimensions of $\boldsymbol{\alpha}^*$ in Fig. 8. The horizontal coordinate of the gray line represents the estimated noisy standard variance. And the absolute value of α_j^* is presented by the bar chart. The experiment is conducted on the first task of Aircraft-B0Inc10 setting. Results show that 98.14% of the α_j^* satisfy the condition of $\sigma^2 \geq (\alpha_j^*)^2$ and 99.9% of the α_j^* satisfy the condition of $\sigma^2 \geq 2\lambda(\alpha_j^*)^2$ with $\lambda = 0.1$. Therefore, when d_j takes an appropriate value, $\sigma^2 \geq (2\lambda + d_j^2)(\alpha_j^*)^2$ can be satisfied.

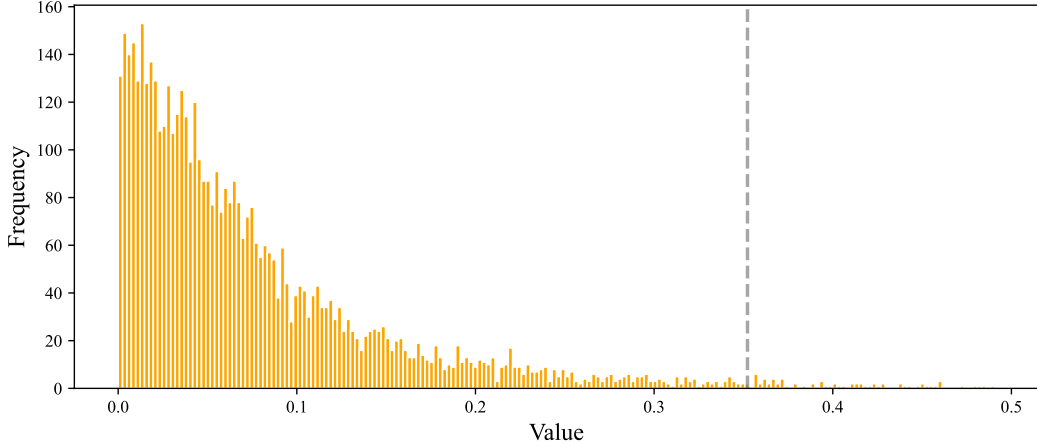


Figure 8: The estimated noisy variance (gray line) and the bar chart for the absolute value of α_j^* on the first task of Aircraft-B0Inc10 setting.

F ANALYTIC CIL WITH WEIGHT ADJUSTMENT.

In this section, we derive how to get the closed-form solution of ridge regression with re-weight in the incremental learning setting. The derivation of the standard ridge regression can be seen as setting the weight matrix to the identity matrix. The optimization objective of ridge regression with weight can be reformed as:

$$\begin{aligned} \mathcal{L}(\mathbf{W}_T) &= (\mathbf{X}_{1:T}\mathbf{W}_T - \mathbf{Y}_{1:T})^\top \mathbf{M} (\mathbf{X}_{1:T}\mathbf{W}_T - \mathbf{Y}_{1:T}) \\ &\quad + \lambda \mathbf{W}_T^\top \mathbf{W}_T, \end{aligned} \tag{34}$$

where $\mathbf{M} = \text{diag}(m_1, \dots, m_n)$ is the diagonal weight matrix.

The gradient w.r.t. \mathbf{W}_T is :

$$\nabla_{\mathbf{W}_T} \mathcal{L} = 2\mathbf{X}_{1:T}^\top \mathbf{M} \mathbf{X}_{1:T} \mathbf{W}_T - 2\mathbf{X}_{1:T}^\top \mathbf{M} \mathbf{Y}_{1:T} + 2\lambda \mathbf{W}_T \tag{35}$$

Setting gradient to zero:

$$\begin{aligned} \hat{\mathbf{W}}_T &= (\mathbf{X}_{1:T}^\top \mathbf{M} \mathbf{X}_{1:T} + \lambda \mathbf{I})^{-1} \mathbf{X}_{1:T}^\top \mathbf{M} \mathbf{Y}_{1:T} \\ &= \left([\mathbf{X}_1^\top \cdots \mathbf{X}_T^\top] \begin{bmatrix} \mathbf{M}_1 & \cdots & \mathbf{0} \\ \vdots & \ddots & \vdots \\ \mathbf{0} & \cdots & \mathbf{M}_T \end{bmatrix} \begin{bmatrix} \mathbf{X}_1 \\ \vdots \\ \mathbf{X}_T \end{bmatrix} + \lambda \mathbf{I} \right) [\mathbf{X}_1^\top \cdots \mathbf{X}_T^\top] \begin{bmatrix} \mathbf{M}_1 & \cdots & \mathbf{0} \\ \vdots & \ddots & \vdots \\ \mathbf{0} & \cdots & \mathbf{M}_T \end{bmatrix} \begin{bmatrix} \mathbf{Y}_1 \\ \vdots \\ \mathbf{Y}_T \end{bmatrix} \\ &= \left(\sum_{t=1}^T \mathbf{X}_t^\top \mathbf{M}_t \mathbf{X}_t + \lambda \mathbf{I} \right)^{-1} \left(\sum_{t=1}^T \mathbf{X}_t^\top \mathbf{M}_t \mathbf{Y}_t \right) \end{aligned} \tag{36}$$

where \mathbf{M}_t is the diagonal weight matrix of \mathbf{X}_t . Then the closed-form solution for \mathbf{W}_T can be updated recursively as:

$$\hat{\mathbf{W}}_T = (\mathbf{A}_T + \lambda \mathbf{I})^{-1} \mathbf{C}_T, \tag{37}$$

with

$$\mathbf{A}_t = \mathbf{A}_{t-1} + \mathbf{X}_t^\top \mathbf{M}_t \mathbf{X}_t, \quad \mathbf{C}_t = \mathbf{C}_{t-1} + \mathbf{X}_t^\top \mathbf{M}_t \mathbf{Y}_t. \tag{38}$$

G DETAILED PERFORMANCE ON EACH TASKS

To present the results in detail, we present the accuracy of different methods with e LAION-400M pre-trained CLIP ViT-B/16 after different tasks in Fig. 9 (without base classes) and Fig. 10 (with

base classes). Unlike the typical declining trend of accuracy across tasks, we observe an increasing accuracy trajectory on certain datasets. This phenomenon stems from varying difficulties in generating pseudo labels for unlabeled data at different stages, when higher quality pseudo labels are produced, the performance improves accordingly. Notably, our method achieves the best performance on nearly all tasks. This is attributed to our proposed pseudo label refinement strategy, which effectively refines noisy labels, as well as the intra-class and inter-class adjustment methods that mitigate class frequency imbalance and leverage confidence information from pseudo labels.

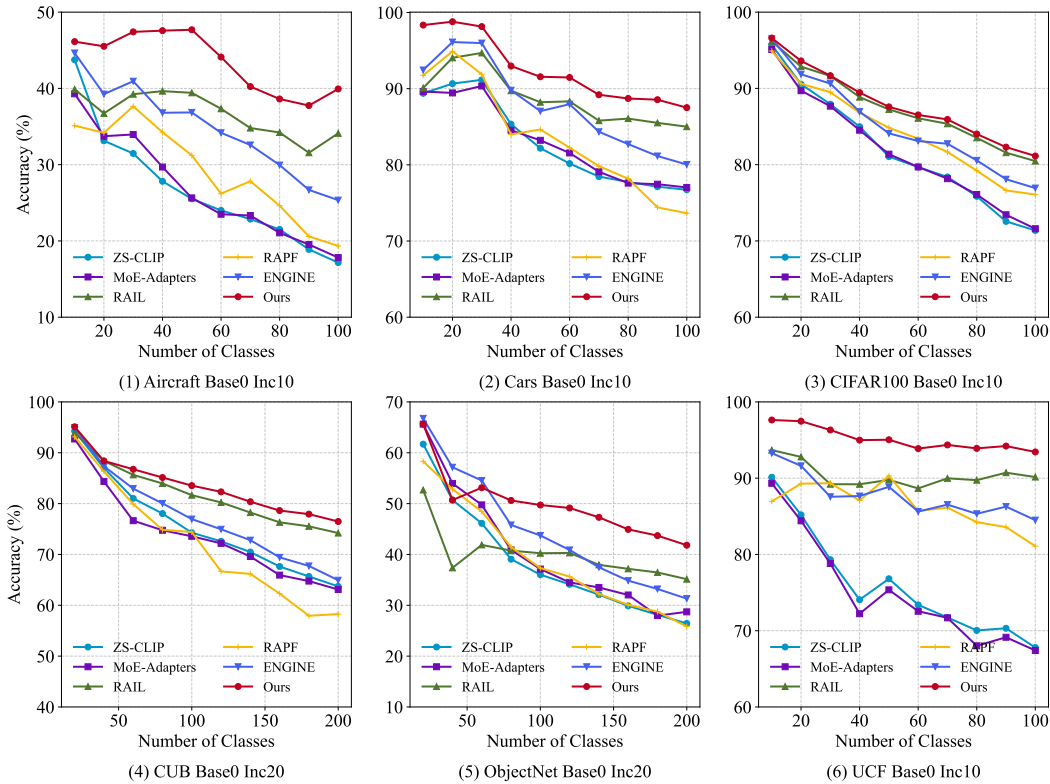


Figure 9: Results of each task without base classes.

H PSEUDO CODE

We provide the pseudo code in Algorithm 1. For task t , we first obtain the image features X_t and the pseudo labels \tilde{Y}_t . As described in the first paragraph of Sec. 3.4, the projected features $X_{t,k}$ together with \tilde{Y}_t are used to perform a regression step that yields a refined classifier \hat{W}'_t . The refined pseudo labels \tilde{Y}'_t are then computed according to Eq. 4. We replace the original pseudo labels \tilde{Y}_t with \tilde{Y}'_t to enable progressive label refinement. After the refinement, the classification head for continual learning is trained using X_t , the latest refined labels \tilde{Y}'_t , and the bi-level weight adjustment strategy.

I MORE RESULTS

I.1 STATISTICAL RESULTS

Besides the reported mean results reported in Table 1, we also report standard deviation across three independent runs in Table 7. These statistical results show that our method maintains stable performance across different runs, demonstrating its robustness.

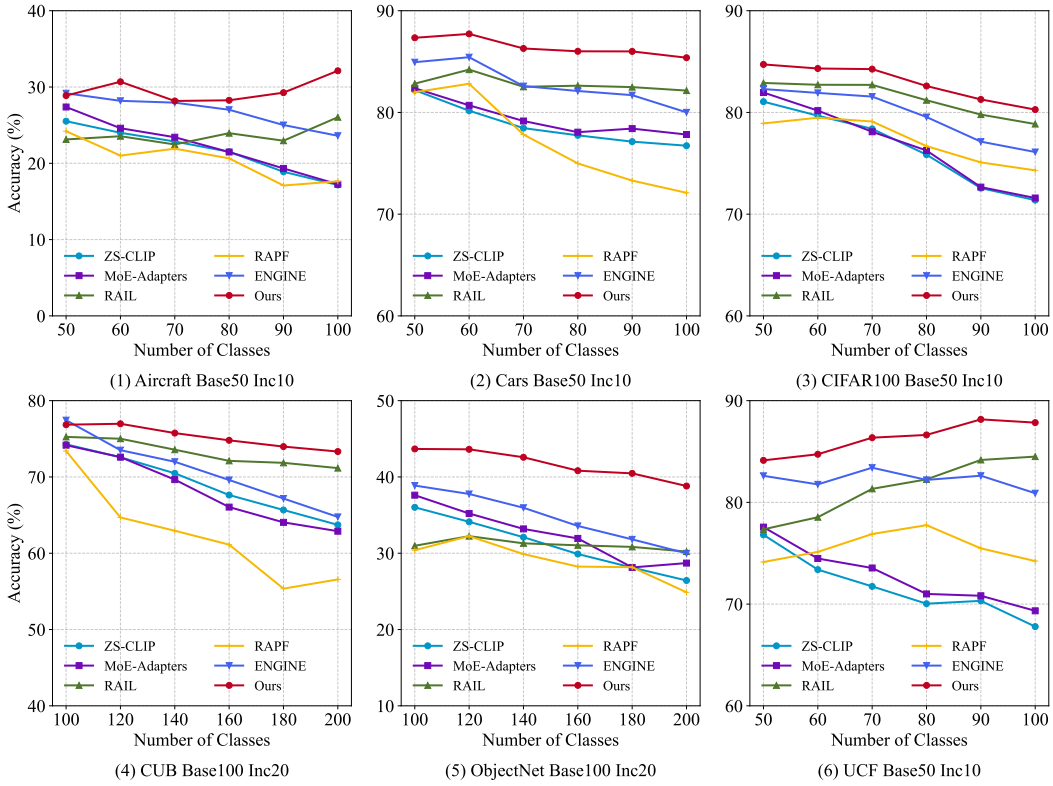


Figure 10: Results of each task with base classes.

Table 7: The mean and standard deviation results of N2L.

Method	Aircraft				Cars				CIFAR100			
	B0Inc10 $\bar{\mathcal{A}}$	B50Inc10 \mathcal{A}_B	B0Inc10 $\bar{\mathcal{A}}$	B50Inc10 \mathcal{A}_B	B0Inc10 $\bar{\mathcal{A}}$	B50Inc10 \mathcal{A}_B	B0Inc10 $\bar{\mathcal{A}}$	B50Inc10 \mathcal{A}_B	B0Inc10 $\bar{\mathcal{A}}$	B50Inc10 \mathcal{A}_B	B0Inc10 $\bar{\mathcal{A}}$	B50Inc10 \mathcal{A}_B
N2L	43.73 ± 0.24	40.21 ± 0.20	29.69 ± 0.24	32.42 ± 0.26	92.38 ± 0.14	87.50 ± 0.15	86.42 ± 0.02	85.45 ± 0.09	87.80 ± 0.10	81.13 ± 0.03	82.92 ± 0.03	80.30 ± 0.04
CUB												
Method	ObjectNet				UCF							
	B0Inc20 $\bar{\mathcal{A}}$	B100Inc20 \mathcal{A}_B	B0Inc20 $\bar{\mathcal{A}}$	B100Inc20 \mathcal{A}_B	B0Inc20 $\bar{\mathcal{A}}$	B100Inc20 \mathcal{A}_B	B0Inc20 $\bar{\mathcal{A}}$	B100Inc20 \mathcal{A}_B	B0Inc10 $\bar{\mathcal{A}}$	B50Inc10 \mathcal{A}_B	B0Inc10 $\bar{\mathcal{A}}$	B50Inc10 \mathcal{A}_B
N2L	83.41 ± 0.07	76.48 ± 0.05	75.16 ± 0.08	73.40 ± 0.10	49.31 ± 0.35	41.59 ± 0.20	41.42 ± 0.24	38.65 ± 0.26	95.00 ± 0.10	93.29 ± 0.21	86.41 ± 0.08	87.87 ± 0.03

I.2 MORE ABLATION RESULTS

In the main paper, we present a subset of the results in Fig. 4 to maintain readability. Additional results for each individual component are provided in Table. 8. When incorporating only a single component, the pseudo-label refinement module achieves the most significant improvement. The inter-class and intra-class adjustment modules further enhance performance by balancing the weights of different samples. Finally, combining all components yields the best overall results.

I.3 NOISY TASK BOUNDARY

In this section, we evaluate our approach under a noisy task boundary scenario, where 20% or 50% of the training samples are drawn from $C_{1:t-1}$. The results in Table. 9 show that our N2L still outperforms existing methods under such noisy conditions, demonstrating its effectiveness.

Algorithm 1 N2L Training Procedure

Input: Pre-trained VLM $\mathcal{V} = (f_{\text{img}}, f_{\text{text}})$; data stream $\mathcal{D} = \{\mathcal{D}_t\}_{t=1}^T$ where $\mathcal{D}_t = \{\mathcal{U}_t, \mathcal{C}_t\}$; regularization λ .

Output: Incremental classifier $\hat{\mathbf{W}}_T$.

```

1: Initialize  $\mathbf{A}_0 = \mathbf{0}$ ,  $\mathbf{C}_0 = \mathbf{0}$ .
2: for  $t = 1$  to  $T$  do
3:   Step 1: Pseudo Label Generation
4:   for each  $x_i \in \mathcal{U}_t$  do
5:     Compute  $\tilde{y}_i = \arg \max_{c \in \mathcal{C}_t} \langle f_{\text{img}}(x_i), f_{\text{text}}(p_c) \rangle$  (Eq. 1)
6:   end for
7:   Form pseudo-label matrix  $\tilde{\mathbf{Y}}_t$ .
8:
9:   Step 2: Progressive Label Refinement
10:  Extract visual features  $\mathbf{X}_t$ .
11:  Compute SVD:  $\mathbf{X}_t = \mathbf{U}\mathbf{D}\mathbf{V}^\top$ .
12:  Select top- $k$  singular vectors above threshold  $\theta$ :  $\mathbf{V}_k$ .
13:  Project features:  $\mathbf{X}_{t,k} = \mathbf{X}_t \mathbf{V}_k$ .
14:  for iter = 1 to refinement steps do
15:    Learn refinement classifier  $\hat{\mathbf{W}}'_t$  using  $(\mathbf{X}_{t,k}, \tilde{\mathbf{Y}}_t)$  and weight adjustment.
16:    Update labels  $\tilde{\mathbf{Y}}_t = \arg \max(\mathbf{X}_{t,k} \hat{\mathbf{W}}'_t)$ . (Eq. 5)
17:  end for
18:
19:   Step 3: Bi-level Weight Adjustment
20:   Compute class-frequency weights  $m_{\text{inter}}$ . (Eq. 7)
21:   Compute entropy  $E$  from logits  $\mathbf{X}_{t,k} \hat{\mathbf{W}}'_t$ . (Eq. 9)
22:   Sample intra-class weights from  $\mathcal{N}(1, \sigma^2)$ , sort and reorder by entropy.
23:   Compute weights  $m_i = m_{\text{inter},i} \cdot m_{\text{intra},i}$ . (Eq. 10)
24:   Form diagonal weight matrix  $\mathbf{M}_t$ .
25:
26:   Step 4: Recursive Analytic CIL Update
27:   Update sufficient statistics: (Eq. 13)

```

$$\mathbf{A}_t = \mathbf{A}_{t-1} + \mathbf{X}_t^\top \mathbf{M}_t \mathbf{X}_t, \quad \mathbf{C}_t = \mathbf{C}_{t-1} + \mathbf{X}_t^\top \mathbf{M}_t \tilde{\mathbf{Y}}_t.$$

28: Compute incremental classifier: (Eq. 12)

$$\hat{\mathbf{W}}_t = (\mathbf{A}_t + \lambda \mathbf{I})^{-1} \mathbf{C}_t.$$

29: **end for**

Table 8: More ablation results of N2L.

Aircraft-B0Inc10	$\bar{\mathcal{A}}$	\mathcal{A}_B
Base	36.23	33.59
Base+Intra	37.29	34.35
Base+Inter	37.31	35.31
Base+Refine	39.50	35.64
Base+Inter+Intra	38.14	36.45
Base+Intra+Refine	41.17	36.17
Base+Inter+Refine	42.34	39.66
Base+Inter+Intra+Refine	43.73	40.21

J INFERENCE STEP

During inference, we follow the prediction fusion strategy of RAIL (Xu et al., 2024), which computes the final output by taking a weighted sum of the zero-shot CLIP logits and the logits produced by the

Table 9: Results of different methods under a noisy task boundary scenario, where 0%, 20% or 50% of the training samples at task t are drawn from previous tasks.

Method	Aircraft				Cars				CIFAR100			
	B0Inc10		B50Inc10		B0Inc10		B50Inc10		B0Inc10		B50Inc10	
	\bar{A}	\mathcal{A}_B										
RAIL(0%)	36.23	33.59	23.75	25.99	88.64	84.68	82.72	82.13	87.34	80.37	81.44	78.89
ENGINE(0%)	34.77	25.41	26.94	23.56	86.90	78.76	82.67	79.93	85.15	77.11	79.89	76.15
N2L(0%)	43.73	40.21	29.69	32.42	92.38	87.50	86.42	85.45	87.80	81.13	82.92	80.30
RAIL(20%)	35.19	31.71	23.06	24.60	87.95	82.81	82.37	81.02	87.01	79.95	81.10	78.38
ENGINE(20%)	33.95	24.72	26.51	22.56	86.45	78.32	82.16	79.18	84.72	76.61	79.52	75.86
N2L(20%)	43.11	38.70	29.13	30.51	91.06	85.26	86.00	84.23	87.68	80.81	82.78	80.07
RAIL(50%)	33.46	28.83	21.97	21.81	85.56	78.74	81.52	78.99	86.55	79.20	80.67	77.69
ENGINE(50%)	33.36	23.25	25.63	21.39	85.44	76.56	80.83	75.90	83.72	75.68	78.64	74.50
N2L(50%)	40.49	36.00	27.45	27.75	89.32	81.61	85.10	81.58	87.02	80.27	82.39	79.23
<hr/>												
Method	CUB				ObjectNet				UCF			
	B0Inc20		B100Inc20		B0Inc20		B100Inc20		B0Inc10		B50Inc10	
	\bar{A}	\mathcal{A}_B										
RAIL(0%)	81.64	73.93	73.08	70.91	39.80	35.13	31.21	30.19	90.18	89.90	81.05	84.27
ENGINE(0%)	77.06	65.07	70.85	64.92	44.57	31.24	34.62	29.96	87.85	84.46	82.30	81.04
N2L(0%)	83.41	76.48	75.16	73.40	49.31	41.59	41.42	38.65	95.00	93.29	86.41	87.87
RAIL(20%)	80.25	71.61	72.72	70.02	38.61	33.66	30.29	28.74	88.54	88.33	80.45	83.21
ENGINE(20%)	75.68	63.60	70.20	64.19	44.01	30.34	34.28	29.39	86.94	84.54	82.04	80.64
N2L(20%)	82.10	74.28	74.46	71.76	48.10	40.84	40.96	37.73	93.15	91.21	85.85	86.43
RAIL(50%)	78.38	68.45	71.20	66.33	34.48	29.53	28.09	24.98	86.31	85.75	78.44	79.58
ENGINE(50%)	74.39	61.79	69.22	62.82	42.72	29.75	33.53	28.41	84.28	82.83	80.75	78.63
N2L(25%)	79.86	70.52	72.80	68.54	46.48	37.09	39.05	34.94	90.80	88.86	84.75	84.99

learned classification head. Specifically, the final logit for sample i , denoted as $Y_{i,\text{final}}$, is computed as:

$$Y_{i,\text{final}} = (1 - \beta) \tilde{Y}_i + \beta Y_i \quad (39)$$

where \tilde{Y}_i is the logit predicted by N2L, Y_i is the zero-shot CLIP logit, β is a weighting parameter set to 0.2 following RAIL.